Assessing impacts of coastal warming, acidification, and deoxygenation on Pacific oyster (*Crassostrea gigas*) farming: A case study in the Hinase Area, Okayama Prefecture and Shizugawa Bay, Miyagi Prefecture, Japan

Masahiko Fujii[1,2,3], Ryuji Hamanoue[2], Lawrence Patrick Cases Bernardo[1,3], Tsuneo Ono[3,4], Akihiro Dazai[5,4], Shigeyuki Oomoto[6,5], Masahide Wakita[7,6], and Takehiro Tanaka[8,7]

[1]International Coastal Research Center, Atmosphere and Ocean Research Institute, The University of Tokyo, Iwate, 0281102, Japan
Faculty of Earth Environmental Science, Hokkaido University, Sapporo, 0600810, Japan
[2]Graduate School of Environmental Science, Hokkaido University, Sapporo, 0600810, Japan
[3]Now at International Coastal Research Center, Atmosphere and Ocean Research Institute, The University of Tokyo, Iwate, 0281102, Japan
[4]Fisheries Resources Institute, Japan Fisheries Research and Education Agency, Yokohama, 2368648, Japan
[4,5]Center for Sustainable Society, Minamisanriku, 9860775, Japan
[5,6]Eight-Japan Engineering Consultants Inc., Okayama, 7008617, Japan
[6,7]Mutsu Institute for Oceanography, Japan Agency for Marine-Earth Science and Technology, Aomori, 0350022, Japan
[7,8]NPO Satoumi Research Institute, Okayama, 7048194, Japan

Correspondence to: Masahiko Fujii (mfujii@aori.u-tokyo.ac.jp)

Abstract. Coastal warming, acidification, and deoxygenation are progressing primarily due to the increase in anthropogenic CO_2. Coastal acidification has been reported to have effects that are anticipated to become more severe as acidification progresses, including inhibiting the formation of shells of calcifying organisms such as shellfish, which include Pacific oysters (*Crassostrea gigas*), one of the most important aquaculture resources in Japan. Moreover, there is concern regarding the combined impacts of coastal warming, acidification, and deoxygenation on Pacific oysters. However, spatiotemporal variations in acidification and deoxygenation indicators such as pH, aragonite saturation state (Ω_{arag}), and dissolved oxygen have not been observed and projected in oceanic Pacific oyster farms in Japan. To assess the present and project future impacts of coastal warming, acidification, and deoxygenation on Pacific oysters, we performed continuous *in-situ* monitoring, numerical modeling, and microscopic examination of Pacific oyster larvae in the Hinase area of Okayama Prefecture and Shizugawa Bay in Miyagi Prefecture, Japan, both of which are famous for their Pacific oyster farms. Our monitoring results first found Ω_{arag} values lower than the critical level of acidification for Pacific oyster larvae in Hinase, although no impact of acidification on larvae was identified by microscopic examination. Our modeling results suggest that Pacific oyster larvae are anticipated to be affected more seriously by the combined impacts of coastal warming and acidification, with lower pH and Ω_{arag} values and a prolonged spawning period, which may shorten the oyster shipping period and lower the quality of oysters. ~~On the other hand, no significant impact of surface-water deoxygenation on Pacific oysters was identified at present nor was projected for the future in both sites.~~

1 Introduction

Since the industrial revolution of the mid-18th century, anthropogenic carbon dioxide (CO_2) emissions have increased (Intergovernmental Panel on Climate Change (IPCC), 2021) as a result of activities such as fossil-fuel consumption, industry, and land-use changes (e.g. Le Quéré et al., 2018). The CO_2 emitted has a greenhouse effect and is therefore a contributor to global warming. Global warming is progressing due to the increase in anthropogenic CO_2 and other greenhouse gases. In addition, ocean temperatures are increasing as the oceans absorb the increased thermal energy associated with global warming (e.g. Levitus et al., 2009).-There is concern that the impact on ecosystems in the seas will be considerable. The effects of rising sea temperatures on ecosystems vary. Most marine organisms are heterotherms, and there have been reports at higher latitudes of organisms that usually prefer warmer seawater in the south. Global warming may also cause extreme events such as larger typhoons (e.g. Yoshino et al., 2015) and increased heavy rainfall (e.g. Papalexiou and Montanari, 2019). Increased high- rainfall events result in increased river flooding and alter material inputs to the ocean, thus affecting coastal ecosystems (Hoshiba et al., 2021), which may, in turn, affect human well-being via fisheries and marine tourism. Therefore, it is necessary to predict the impact of ocean warming on coastal areas and ecosystems, and to implement appropriate adaptation measures.

CO_2 absorbed by the oceans from the atmosphere~~leached into the ocean~~ reacts with water (H_2O) in seawater to form carbonic acid (H_2CO_3), and the H_2CO_3 separates into hydrogen ions (H^+), bicarbonate ions (HCO_3^-), and carbonate ions (CO_3^{2-}), releasing H^+into seawater:

$$CO_2 + H_2O \rightarrow H_2CO_3 \rightarrow HCO_3^- + H^+. \quad (1)$$

Therefore, as the amount of CO_2 absorbed by~~leached into~~ the ocean increases, seawater, which is inherently slightly alkaline, decreases in pH and becomes closer to neutral or acidic. This phenomenon is called ocean acidification (Orr et al., 2005; Bates et al., 2014; Jiang et al., 2019).

Ocean acidification is a global phenomenon. Over the past century, global average pH values have decreased by 0.1 unit, indicating an increase in hydrogen ion concentrations ($[H^+]$) of nearly 30% (Orr et al., 2005; Doney et al., 2020). Additionally, rates of ocean acidification have been reported to vary by region, especially in coastal regions. A major contributor to the differences in the progression of acidification in coastal areas is human activity, such as coastal protection works, inflows of river water containing industrial wastewater, and sea-surface aquaculture (Suzuki et al., 2020). In addition, spatiotemporal variations in seawater pH are more pronounced in coastal areas than in open-ocean areas because of the complex environments created by natural phenomena such as biological activity and river inflows associated with rainfall. Alterations in the acidity of coastal waters is termed coastal acidification or coastal ocean acidification (Wallace et al., 2014) and is typically distinguished from ocean acidification.

The H^+ in seawater reacts with CO_3^{2-} to maintain equilibrium. Therefore, the concentration of carbonate ions ($[CO_3^{2-}]$) in seawater decreases as acidification progresses. Calcifying organisms such as shellfish, corals, shrimps, and crabs, which have shells and skeletons of calcium carbonate ($CaCO_3$), are affected by this process. Because calcifying organisms form their own shells and skeletons using calcium ions (Ca^{2+}) and CO_3^{2-} in seawater, $CaCO_3$ saturation state (Ω) is an indicator of the effects

on these organisms. Therefore, Ω and pH values are important for evaluating the effects of acidification on organisms. Ω is determined by the product of $[CO_3^{2-}]$ and calcium ion concentration ($[Ca^{2+}]$), which is expressed by the following equation:

$$\Omega = \frac{[Ca^{2+}][CO_3^{2-}]}{K_{sp}}, \quad (2)$$

where K_{sp} is the solubility product of $CaCO_3$ (Guinotte and Fabry, 2008).

Calcifying organisms include commercially important species that provide significant ecosystem services, such as shellfish and corals. Therefore, there are concerns regarding the impact of acidification on human communities. In addition, $CaCO_3$ has two crystalline body structures, aragonite and calcite, with aragonite being the more soluble (Morse et al., 1980). Because the larval stages of shellfish and corals form aragonite shells and skeletons, there is concern that the effects of acidification will be more pronounced than in organisms with calcite shells. Previous studies have reported the effects of reduced aragonite saturation (Ω_{arag}) on different species, based on laboratory experiments that evaluated acidification effects such as coral bleaching and the occurrence of deformities and mortality in larval shellfish by manipulating the partial pressure of CO_2 (Kurihara et al., 2007; Anthony et al, 2008; Kurihara, 2008; Kimura et al., 2011; Onitsuka et al. 2014, 2018; Waldbusser et al., 2015).

Climate change has increased the vertical density gradient of upper-ocean layers, thereby weakening the downward flux of oxygen and hence decreasing the oxygen content. The decreased solubility of oxygen in seawater induced by ocean-surface warming has contributed to the decrease in ocean oxygen content (ocean deoxygenation; Stramma et al., 2010, 2011, 2012, 2020; Helm et al., 2011; Sasano et al., 2015, 2018; Ito et al., 2017; Schmidtko et al., 2017; Oschlies et al., 2018; IPCC, 2019; Ono et al., 2021). In coastal areas, by contrast, oxygen content is frequently disturbed by anthropogenic processes such as eutrophication, changes in freshwater loading, and alteration of topography (coastal deoxygenation; Rabalais et al., 2010; Zhang et al., 2010; Ning et al., 2011; Breitburg et al., 2018; IPCC 2019; Laffoley and Baxter, 2019; Wei et al., 2019; Limburg et al., 2020; Xiong et al., 2020; Fujii et al., 2021; Kessouri et al., 2021). Climate change also affects the coastal oxygen environment by increasing the temperature of coastal water, thus decreasing oxygen solubility, and modulates basin-scale water circulation, thereby changing the patterns and strengths of seasonal intrusions of open-ocean waters into coastal areas (Koslow et al., 2011, 2015; Booth et al., 2012). These indirect consequences of global climate change make coastal oxygen environments more problematic, even if the degree of anthropogenic perturbations in coastal areas remains constant.

In Japan, nutrient loadings from land areas have gradually decreased in most coastal regions (Abo and Yamamoto, 2019). Eutrophic conditions ~~are however~~ still exist~~tant~~ however in many bays and estuaries, and seasonal hypoxic conditions in summer bottom layers improve only slowly (Imai et al., 2006; Ando et al., 2021; Yamamoto et al., 2021). Deoxygenation and ocean acidification cause combined effects on marine organisms (Melzner et al., 2013; DePasquale et al., 2015; Gobler and Baumann, 2016; IPCC, 2018). Monitoring variations in oxygen and pH is thus essential for assessment of conditions in coastal ecosystems.

Pacific oyster farming occupies an important position in the domestic fisheries industry in Japan. In 2018, the value of oyster production from marine aquaculture was about JPY 35 billion, accounting for about 7% of Japan's total marine

aquaculture production. There are concerns regarding the economic impacts of coastal warming, acidification, and deoxygenation on regions where oyster farming is a key industry.

Previous assessments of the effects of acidification on Pacific oysters (*C. gigas*) have shown increased larval mortality and malformation rates due to lower pH and Ω_{arag} values, as well as reduced calcification rates in adult oysters (Gazeau et al., 2007; Kurihara et al., 2007; Waldbusser et al., 2015; Gimenez et al., 2018; Durland et al., 2019). Oyster farms in northwestern Oregon, which generate USD 273 million annually, have been impacted by coastal upwelling causing deep, low-pH, low-Ω_{arag} seawater to manifest at the surface (Barton et al., 2012). There is concern that Japan may face a similar situation in the future as acidification progresses.

Although the ecological effects of coastal warming, acidification, and deoxygenation on Pacific oyster (*C. gigas*) are becoming clearer, when and how these effects will occur at oyster-farming sites are unknown. Because Pacific oyster is a commercially important species, to recommend adaptation measures requires projection of future impacts of coastal warming, acidification, and deoxygenation. For this purpose, we ~~used~~ established monitoring sites in Pacific-oyster-farming areas in Japan and developed a coupled physical-biogeochemical model (Section~~Chapter~~ 2). Section~~Chapter~~ 3 provides observed and modeled~~projected~~ data on coastal warming, acidification, and deoxygenation, and on Pacific oyster and farming thereof. Our findings are discussed and summarized in Sections~~Chapter~~s 4 and 5, respectively.

2 Materials and Methods

2.1 Study sites

Two sites of Pacific oyster (*C. gigas*) aquaculture were selected: the Hinase area (hereafter Hinase) in Bizen City, Okayama Prefecture (Fig. 1(a),(b),(c)) and Shizugawa Bay (hereafter Shizugawa) in Minamisanriku Town, Miyagi Prefecture in the Tohoku region (Fig. 1(a),(d),(e)). Okayama and Miyagi Prefectures together account for approximately 20% of the total domestic oyster aquaculture production, making them important regions for domestic oyster aquaculture. Of these, Hinase accounts for 50% of Okayama Prefecture's oyster aquaculture production, and Shizugawa is a major oyster-farming area, accounting for 10% of Miyagi Prefecture's oyster aquaculture production (Ministry of Agriculture, Forestry and Fisheries website).

Hinase is located in the Seto Inland Sea, the largest enclosed coastal sea in Japan (The Association for Environmental Conservation of the Seto Inland Sea website). The Seto Inland Sea is shallow, with an average depth of 38 m, and is bordered by the open sea at its southeastern, northwestern, and southwestern ends. In addition to being an enclosed sea area, excessive inflow of nutrients from the land due to human activities since the 1950s, loss of seaweed and eelgrass due to land reclamation, and frequent red tides caused by these factors have led to eutrophication of the sea area, and hypoxia and anoxia in the bottom layer. Eutrophication has been overcome in many surface waters of the Seto Inland Sea through measures to control excessive inflow of nutrients from land over the last few decades, and the surface waters are even oligotrophic nowadays (e.g. Abo and

Yamamoto, 2019; Yamamoto et al., 2021), but exchange of seawater with the open sea is weak, and the bottom layer is hypoxic.

Shizugawa Bay is a medium-sized bay that measures approximately 10 km east to west and 5 km north to south, with a mouth facing east (Horii et al., 1994), and has been classified as both an enclosed coastal sea (Ministry of the Environment, 2010) and an open-type bay (Komatsu et al., 2018). Since the 1990s, environmental impacts such as anoxia due to overcrowding of coho salmon and Pacific oysters have been observed (Nomura et al., 1996). Subsequently, the Great East Japan Earthquake of March 11, 2011, caused major damage to the social infrastructure surrounding the bay as well as the aquaculture facilities in the bay, and the subsequent tsunami affected the eelgrass and seaweed beds and tidal flats that support the fisheries.

Against this backdrop, observations of the marine environment are being conducted in both areas, with active cooperation by local fishermen, within the framework of the Nippon Foundation Ocean Acidification Adaptation Project (OAAP; http://nippon.zaidan.info/dantai/0611718/dantai_info.htm), to assess acidification and to develop adaptation measures. Four monitoring sites have been set up in Hinase and Shizugawa (Fig. 1(c),(e)). In Hinase, Site H-1 is located at the mouth of the Chikusa River, the largest river in the study site. Site H-2 is an oyster seedling site, located near the mouth of Katakami Bay. Site H-3 is an eelgrass bed, located at the mouth of Genji Bay. Site H-4 is the farthest offshore, with water depths of 10.2–12.4 m. In Shizugawa, Site S-1 is at the mouth of the Hachiman River, the largest river in the area. Site S-2 is a seaweed-farming site, and Site S-3 is a nursery for oysters. Site S-4 is the farthest offshore, and has water depths of 15.5–16.9 m.

2.2 Observation

We have measured hourly water temperature, salinity, and pH values at a depth of 1 m at each site in Hinase since August 29, 2020 and in Shizugawa since September 4, 2020, using instruments capable of continuous measurement. Dissolved oxygen (DO) has also been monitored continuously at a depth of 1–1.5 m at one site in Hinase (H-2) and one in Shizugawa (S-3) (Fig. 1(c),(e)). A conductivity and temperature sensor (INFINITY-CTW ACTW-USB; JFE Advantech) was used to measure temperature and salinity hourly, while DO was measured hourly using a RINKO W AROW-USB (JFE Advantech). Calibration of the DO sensor was carried out by two-point (zero and span) calibration using 0 and 100% (saturated) oxygen waters (Fujii et al., 2021). To measure pH, glass-electrode pH sensors (SPS-14; Kimoto Electric) were used. The sensors were removed every 1–3 months for cleaning, including removal of attached organisms, data collection, battery replacement, and calibration. See Fujii et al. (2021) for details of the experimental design.

Water samples were collected when the sensors were maintained, and chlorophyll, total alkalinity (TA), dissolved inorganic carbon (DIC), nutrients (nitrate [NO_3], nitrite [NO_2], ammonium [NH_4], phosphate [PO_4], and silicate [Si]) concentrations were measured (Si was not assessed at Shizugawa). TA and DIC values were obtained using a total alkalinitye titration analyzer (ATT-05 by Kimoto Electronic) and a coulometer (Model 3000A; Nippon ANS) (Wakita et al., 2017, 2021; Fujii et al., 2021). The values were calibrated against certified reference material provided by Prof. A. G. Dickson (Scripps Institution of Oceanography, University of California San Diego) and KANSO TECHNOS. The pH (total scale) values at the *in situ* temperatures were calculated from the carbonate dissociation constants in Lueker et al. (2000), the total boron concentration

in Lee et al. (2010), the bisulfate dissociation constant in Dickson (1990), and the hydrogen fluoride dissociation constant in Perez and Fraga (1987), and temperature, salinity, TA, and DIC using CO2SYS (Pierrot et al., 2006).

During continuous monitoring of pH, together with correction of the absolute value, it is necessary to correct for the drift of the sensor~~observed~~ value (Yamaka, 2019; Fujii et al., 2021). In this study, the pH value of a pH sensor at time t (pH(t)) was obtained using the following equation (Hamanoue, 2022):

$$pH(t) = pH_m(t) + [(pH_{sample}(t_i) - pH_m(t_i)) + \{pH_{sample}(t_e) - pH_m(dt_e) - (pH_{sample}(t_i) - pH_m(t_i))\}] \times \frac{t - t_i}{t_e - t_i}, \quad (3)$$

where $pH_m(t)$ represents the measured value of pH at time t; $pH_{sample}(t_e)$ and $pH_{sample}(t_i)$ are the pH values at the end time (t_e) and start time (t_i) of each deployment, respectively, obtained by the seawater sample and sensor; $pH_m(t_i)$ is the pH value measured by the sensor at time t_i; $pH_m(dt_e)$ is the minimal or average pH value measured by the sensor for 24 hours prior to t_e. pH increases during the day due to photosynthesis, and decreases during the night due to respiration of organisms. If algae or other organisms adhere to the glass-electrode portion of the sensor, the effect of photosynthesis during the day is amplified, and the pH value is overestimated. To minimize calibration uncertainty due to this effect, the lowest daily value was used for $pH_m(dt_e)$ if an effect of photosynthesis was observed in the previous 24 hours, and the average value was used if not.

Ω_{arag} can be calculated using two~~one~~ of the following values in addition to water temperature and salinity—pH, TA, DIC, and CO_2 concentration in seawater. Of these, the TA and DIC values were calculated by the above when seawater was sampled, but such sampling was conducted only once or twice per month. Therefore, because the TA of seawater is highly correlated with salinity (e.g. Yamamoto-Kawai et al., 2015), a regression equation was calculated from the salinity and TA values of the seawater samples (Fig. 2(a),(b)). Hourly TA values were estimated from hourly salinity data obtained from continuous observations. Hourly values of Ω_{arag} were calculated using CO2SYS (Lewis et al., 1998), together with water temperature and pH values obtained from continuous observations. The maximum error for this process of determining alkalinity from salinity is about 30 $\mu molkg^{-1}$ and 0.06 for alkalinity and Ω_{arag}, respectively.

To examine the effects of precipitation and freshwater inflow from rivers on the spatiotemporal changes in acidification indices, precipitation data from the sites nearest to Hinase (Mushiage, Oku Town, Setouchi City, Okayama Prefecture) and Shizugawa (Shizugawa, Minamisanriku Town, Miyagi Prefecture, respectively) (Japan Meteorological Agency website; https://www.data.jma.go.jp/obd/stats/etrn/index.php) were obtained. The precipitation data were compared directly with the spatiotemporal changes in salinity, pH, and Ω_{arag} to verify whether variations were due to precipitation or inflow from rivers.

2.3 Microscopic examination of oyster larvae

Like other calcifying organisms, Pacific oyster (*C. gigas*) is particularly vulnerable to acidification at the larval stage. By incubating Pacific oysters in a high-CO_2 tank, Kurihara et al. (2007) revealed that acidified water inhibited the growth of D-shaped veliger larvae. Thus, microscopic examination of D-shaped veliger larvae enables assessment of the impact of acidification on Pacific oyster.

Microscopic examination of D-shaped veliger larvae collected using 50–100-μm mesh plankton nets was carried out in Hinase and Shizugawa during the spawning season. In Hinase, the examination was performed at the Hinase Fisheries Association from July 4 to August 31, 2020 (n = 370) and from June 21 to October 1, 2020 (n = 244), and at the Oku Fisheries Association from July 11 to September 9, 2020 (n = 292), and from July 2 to August 30, 2021 (n = 156). In Shizugawa, microscopy examination was performed at the Kesennuma Miyagi Prefectural Fisheries Experimental Station from July 27 to September 2, 2020 (n = 60) and July 26 to September 6 (n = 70).

2.4 Modeling

To reproduce the coastal environment in Hinase and Shizugawa and to project future conditions, the Regional Ocean Modeling System (ROMS) was used. Of the versions of ROMS, we chose CROCO (ver. 1.1; Jullien et al., 2019), which can perform high-resolution simulations and account for various interactions, including atmosphere, tides, and bathymetry. In addition, CROCO enables coupling of ROMS with the Pelagic Interaction Scheme for Carbon and Ecosystem Studies (PISCES; Aumont et al., 2003; Aumont, 2005), a marine ecosystem model, enabling calculation of biogeochemical as well as physical processes (~~Bernardo et al., 2021;~~ Hamanoue, 2022; Bernardo et al., 2023). The model is therefore suitable for simulating complex coastal marine environments.

The prognostic variables for the physical processes of the model were water temperature and salinity, and those for the biogeochemical processes were DO, TA, DIC, and nutrients (NO_3, PO_4, Si). pH and Ω_{arag} were calculated from the values of water temperature, salinity, TA, and DIC obtained by the model using CO2SYS. The unavoidable biases in model results of prognostic variables relative to observed values were corrected using the procedure adapted by Yara et al. (2011) and Fujii et al. (2021).

The model domain was set to 133° 38' 06" to 135° 47' 67" E and 33° 93' 24" N to 34° 79' 81" in Hinase (Figure 1(b)) and 140° 86' 10" E to 142° 86' 20" E and 37° 59' 47" to 39° 76' 47" N in Shizugawa (Figure 1(d)). The horizontal resolution of the models was approximately 2 km. The vertical coordinate system was σ- coordinate and the number of layers was 32. Bathymetry was derived using the 15 arc-second (~ 500 m near the equator) General Bathymetric Chart of the Oceans (GEBCO) 2021 dataset (GEBCO website; Table 1). Model output data was at 6-hour intervals (Bernardo et al., 2023). Representative simulations were carried out for present and future (2090s) conditions. Each simulation was carried out for a 1-year and 3 month period from May to July~~April~~ (2000 to 2001 for present and 2099 to 2100 for future) and the daily mean results at 1 m depth were used for analysis and comparison with the observed results.

The boundary conditions for water temperature, salinity, current velocity, and water level were taken from the Future Ocean Regional Projection (FORP)-JPN02 version 2 dataset (Nishikawa et al., 2021), which has a horizontal resolution of 2 km, the highest resolution for Japan to date. For the future greenhouse gas emissions scenarios, we used the MRI-CGCM3 climate prediction model outputs developed at the Meteorological Research Institute (Tsujino et al., 2017) under the Representative Concentration Pathways (RCP) 2.6 and 8.5 scenarios (van Vuuren et al., 2011) of the Coupled Model Intercomparison Project phase 5 (CMIP5; Taylor et al., 2012). Table 1 lists the boundary conditions used in this study.

2.5 Thresholds for evaluating the impacts on Pacific oysters (*C. gigas*)

Pacific oysters (*C. gigas*) reach sexual maturity when the accumulated water temperature reaches 600°C based on a water temperature of 10°C, and that at water temperatures of 20°C or higher they spawn once and then mature and spawn again (Oizumi et al., 1971). Therefore, there is a concern that rise in water temperatures in the future may cause earlier or longer spawning and maturation times, which may result in a mismatch with existing oyster-farming approaches. In this study, based on Oizumi et al. (1971), spawning was assumed to start when the accumulated water temperature reaches 600 (℃ day) based on a water temperature of 10 (℃) and to end when the water temperature drops below 20 (℃). There are no previous studies that set the threshold for the impact of ocean acidification on Pacific oysters in Japan coasts. Therefore, to evaluate the impact of ocean acidification on Pacific oysters, we referred to a threshold of Ω_{arag}=1.5 (Waldbusser et al., 2015), which was obtained from rearing experiments of Pacific oyster larvae in Oregon, USA, and hence, the species and reaction to local environment may be different from those in Japan coasts. Below that threshold, the development of Pacific oyster larvae is likely to be affected, with slower growth and higher mortality.

To evaluate the impact of deoxygenation on Pacific oysters, we referred to a threshold ~~of~~ DO concentration of 203 μmol kg^{-1} as a lower limit of the optimal DO range for Pacific oyster growth (Hochachka, 1980; Fisheries Agency, 2013).

3 Results

3.1 Observation results

Water temperatures showed significant seasonal variations at both sites (Fig. 3(a)-(h)). In Hinase, the highest water temperature during the observation period was 32.3°C at H-2 on August 8, 2021 (Fig. 3(b)). The highest water temperatures at the other sites in Hinase were observed on August 2020, with a maximum temperature difference of 1.2°C between sites. The lowest water temperatures were observed in the middle of January, 2021: 6.2°C at H-1, 3.9°C at H-2, 5.6°C at H-3, and 7.3°C at H-4 (Fig. 3(a)-(d)). In Shizugawa, the highest water temperature during the observation period was 28.7°C at S-2 on August 6, 2021 (Fig. 3(f)), and the highest water temperatures at the other sites were observed on September 8, 2020 or August 6, 2021 (Fig. 3(e), (g), (h)). The lowest water temperature of 6.5°C was observed at S-1 on February 9, 2021 (Fig. 3(e)). The difference between sites was about 0.8°C and 0.7°C for the maximum and minimum water temperatures, respectively.

As mentioned in 2.5, spawning periods of Pacific oysters are estimated from the water temperature thresholds based on Oizumi et al. (1971). In Hinase, Pacific oysters ~~are~~ were estimated to have stopped spawning between October 24 and November 4, 2020, and between October 25 and November 7, 2021 and to have begun spawning between June 8 and 19 in 2021. In Shizugawa, spawning ~~is~~ was estimated to have ended between October 8 and 10, 2020 and between October 16 and

18, 2021, and to have begun between July 19 and 24, 2021 (Table 2).

Salinity usually varied between 30.5 and 31.5 at sites in Hinase and between 32 and 34 in Shizugawa (Fig. 3(i)-(p)). In the Hinase Area, the minimum salinity at H-1, H-2, H-3, and H-4 during the monitoring period was 11.4, 13.3, 16.5, and 15.3, and appeared on July 9, August 23, July 10, and July 10, 2021, respectively (Fig. 3(i)-(l)). The lowest salinity at H-1, H-3, and H-4 appeared on July 9-10 and the second lowest salinity at H-2 during the monitoring period (15.4) also appeared on July 11, 2021 (Fig. 3(j)), and the heaviest rainfall during the monitoring period (hourly precipitation of 28.5 mm) around the sites occurred at 4 am on July 8, 2021, i.e., one or two days before the lowest salinity appeared at the sites. The lowest salinity at H-2 appeared on August 23, 2021, after intermittent rainfall which lasted for several days from August 12, 2021. In the Shizugawa Bay, the minimum salinity at S-1, S-2, S-3, and S-4 during the monitoring period was 15.2, 23,5, 27.9, and 28.8, and appeared on September 5, 2020, August 23, 2020, May 2, 2021, and July 11, 2021, respectively (Fig. 3(m)-(p)). The extremely low salinity observed~~appeared~~ at S-1 (located at the mouth of the Hachiman River) at 5 pm on September 5, 2020 (Fig. 3(m))~~,~~ seemed to be caused by the heaviest rainfall during the monitoring period, which was recorded on that day (hourly precipitation of 37.5 mm at 8am; 9 hours earlier than the appearance of the lowest salinity at S-1)~~;~~, presumably the increased freshwater discharge from the Hachiman River followed~~ing~~ the heavy rainfall. Although the relation between the salinity and rainfall ~~in~~ during the entire period of monitoring was not statistically significant at any of the sites in Hinase and Shizugawa, extremely low salinity seems to be related to direct freshwater input from the rainfall and subsequently increased freshwater discharge from nearby~~vicinal~~ rivers. Rainfall does not always result in a significant decrease in salinity, but when there is a significant decrease in salinity, it always tends to be after rainfall events.

The observed nutrient concentrations differed among sites and had large seasonal and interannual fluctuations, being relatively high in late summer and autumn, and low in the other periods (not shown). The observed range of NO_3 concentration was 0.01-8.18 μmol kg^{-1} in Hinase and 0.00-4.75 μmol kg^{-1} in Shizugawa. That of PO_4 concentration was 0.03-1.29 μmol kg^{-1} in Hinase and 0.01-0.74 μmol kg^{-1} in Shizugawa. It is difficult to assess if the waters are oligotrophic or not by certain thresholds of nutrient concentrations. On the other hand, if we refer to the half-saturation constant of each nutrient concentration given in the model (e.g. 0.26-1.3 μmol kg^{-1} for NO_3 and 0.0008-0.004 μmol kg^{-1} for PO_4 in Aumont (2005)), NO_3 and PO_4 are considered to be depleted which is regarded as oligotrophic condition in some seasons in the surface water in both sites.

DO concentrations showed significant seasonal variation, generally being high in winter and low in summer at all sites in Hinase (Fig. 4(a) and Shizugawa (Fig. 4(b)). Although the DO concentrations were above the lower limit of the optimal DO range for Pacific oyster growth (203 μmol kg^{-1}; Hochachka, 1980; Fisheries Agency, 2013) in Shizugawa, they were often below the optimal range in summer and autumn in Hinase.

TA values estimated from continuous salinity observations using the above-mentioned regression equation (Fig. 2) matched those determined by water-sample analysis at each site (Fig. 5(a)-(h)). The estimates implied a significant decrease in TA values, associated with a localized decrease in salinity as a result of rainfall and subsequent enhanced riverine discharge, that could not be captured by once-or twice-monthly water-sample analysis.

DIC values determined by water-sample analysis showed clear seasonal variation, being generally high in winter and low in summer (Fig. 5(i)-(p)), likely a result of the higher solubility of atmospheric CO_2 at low temperatures and more vigorous primary production, respectively. The DIC estimated from water temperature, salinity, and pH (and TA via salinity) showed similar fluctuations to the corresponding TA. In~~By~~ contrast, the estimated DIC showed abrupt changes at all sites that were not captured by water-sample analysis. Abrupt drawdowns of estimated DIC were sometimes found, and a significant decrease occurred at all four sites in Hinase on July 13, 2021 (Fig. 5(i)-(l)), after a major rainfall event.

pH values varied widely during the observation period at all sites in Hinase and Shizugawa, with a marked decrease after rainfall (Fig. 6(a)-(h)). The extent of the post-rainfall decline in pH differed among the sites. In Hinase, the lowest pH was in September 2021 (Fig. 6(a)-(d)), and pH values were lower at H-1, H-2, and H-3 than at H-4, which was the farthest offshore. After rainfall on September 2021, the lowest pH values at H-1 and H-2 were 0.2 units lower than those at the other two sites. In Shizugawa, the lowest pH value of 7.8 occurred in July and August 2021, at S-1 and S-3 (in the estuary and offshore, respectively) (Fig. 6(e), (g)).

Ω_{arag} varied significantly during the observation period at all sites in Hinase and Shizugawa (Fig. 6(i)-(p)). The temporal variability varied from site to site, with greater decreases at sites closer to the coast. Ω_{arag} values < 1.5 were often detected in Hinase, especially at H-1 and H-2 (Fig. 6(i), (j)), which were close to the river. Furthermore, during the spawning season of Pacific oysters from June to October or November (Oizumi et al., 1971), values fell below that threshold locally; the lowest Ω_{arag} of 0.8 was observed at H-2, which is used as a nursery for oysters, and values remained below the threshold for 2 weeks (Fig. 6(j)). In Shizugawa, the Ω_{arag} value was below the threshold only in August 2021 at S-3 for 4 hours (Fig. 6(o), (p)), coinciding with the spawning season of Pacific oysters. However, no morphological abnormalities were observed in the larvae from Hinase and Shizugawa (Fig. 7), and therefore, we did not find any anecdotal evidence of impacts of ocean acidification on Pacific oyster larvae in this study.

3.2 Modeling results

The model successfully reproduced the spatio-temporal variations of each parameter in Hinase and Shizugawa (Figs. 8 and 9), such as significant seasonal fluctuation of water temperature (Figs. 8(a)-(d), 9(a)-(d)). The modeled salinity was relatively uniform in space and season. However, the salinity was lower in coastal regions in Hinase, especially near rivers in summer where and when freshwater discharge from rivers are dominant (Fig. 8(e)-(h)). The spatio-temporal variability was less in Shizugawa, although the seawater flowing into the bay is likely influenced by freshwater discharged from the Kitakami River, the fifth longest river in Japan (Fig. 9(e)-(h)). The modeled DO is in direct contraset with water temperature, higher in winter and lower in summer (Figs. 8(i)-(l) and 9(i)-(l)), primarily caused by higher and lower solubility of oxygen in cooler and warmer water, respectively.

The modeled temperature reproduced the observed seasonal fluctuations in Hinase (Fig. 10(a)-(d)) and Shizugawa (Fig. 10(e)-(h)). However, the modeled seasonal fluctuation of temperature was around 1 month behind observations in Shizugawa.

The model–observations~~data~~ mismatch may be a result of the internal variability of the climate model (Yara et al., 2011), especially for the Pacific Ocean, which provided the boundary conditions used in this study. Nonetheless, based on Oizumi et al. (1971), the current start and end date of Pacific oyster's spawning period was calculated to be on June 14 in Hinase and July 26 in Shizugawa, and on October 24 in Hinase and October 14 in Shizugawa, respectively. These are consistent with the observation-based estimated start dates (June 8-19 in Hinase and July 19-24 in Shizugawa) and end dates (October 24-November 7 in Hinase and October 8-18 in Shizugawa), respectively (Table 2). The observed sudden decrease in the salinity was reproduced but was underestimated by the model (Fig. 10(i)-(p)).

The modeled DO, TA, and DIC values reproduced the observed seasonal fluctuations in Hinase and Shizugawa (Figs. 11(a)-(b) and 12(a)-(p)). However, the model did not reproduce the short-term fluctuations in biogeochemical parameters. This was mainly because the temporal resolution of the model output is 6 hours~~1 day~~, insufficient to resolve significant short-term~~daily~~ fluctuations in biogeochemical processes predominantly caused by biological activities, i.e., photosynthesis by phytoplankton, eelgrass, and seaweeds during the day and respiration of marine organisms~~creatures~~ at night. Although the spatial resolution of the model (2 km) is relatively high for downscaling climate model outputs, it is insufficient to reproduce spatial differences in biogeochemical-parameter values among the four sites in Hinase and Shizugawa. Also, the model-observations~~data~~ mismatch for TA and DIC values, especially the failure to reproduce sudden decreases, likely resulted from insufficient input of freshwater from rainfall and riverine water into the model.

The modeled pH and Ω_{arag} values reproduced those observed (Fig. 13(a)-(p)). However, similar to the other biogeochemical parameters, the model had difficulty in simulating short-term fluctuations. Because the model's pH and Ω_{arag} values are calculated from modeled temperature, salinity, TA, and DIC values, uncertainties in the latter could magnify or cancel out those in the former. The estimated number of days on which Ω_{arag} values are below the threshold of acidification for Pacific oyster larvae (1.5) at present by the model results is 0 days in both Hinase and Shizugawa. The number of days is modified to 3 days in Hinase and 7 days in Shizugawa, respectively, if the observed short-term fluctuation is taken into account~~12 days in Hinase and 0 days in Shizugawa~~ (Table 3).

Following previous studies (e.g. Hauri et al., 2013; DeJong et al., 2015; Wada et al., 2020), monthly-mean contributions of pH and Ω_{arag} changes (ΔpH and $\Delta\Omega_{arag}$, respectively) with temperature (∂pH/∂T * ΔT and $\partial\Omega_{arag}$ /∂T * ΔT), TA (∂pH/∂TA * ΔnTA and $\partial\Omega_{arag}$ /∂TA * ΔnTA), DIC (∂pH/∂DIC * ΔnDIC and $\partial\Omega_{arag}$ /∂DIC * ΔnDIC), and salinity (ΔFSpH and ΔFSΩ_{arag}) during the study period were examined. The c~~C~~ontribution of ΔpH and $\Delta\Omega_{arag}$ in each parameter is expressed as follows, based on Hauri et al. (2013):

$$\Delta pH \cong \frac{\partial pH}{\partial T}\Delta T + \frac{\partial pH}{\partial TA}\Delta nTA + \frac{\partial pH}{\partial DIC}\Delta nDIC + \Delta FS_{pH}, \quad (3)$$

and

$$\Delta\Omega_{arag} \cong \frac{\partial \Omega_{arag}}{\partial T}\Delta T + \frac{\partial \Omega_{arag}}{\partial TA}\Delta nTA + \frac{\partial \Omega_{arag}}{\partial DIC}\Delta nDIC + \Delta FS_{\Omega_{arag}}, \quad (4)$$

where

$$\Delta FS_{pH} = \frac{\partial pH}{\partial S}\Delta S + \frac{\partial pH}{\partial TA}\Delta TA^S + \frac{\partial pH}{\partial DIC}\Delta DIC^S, \quad (5)$$

and

$$\Delta FS_{\Omega_{arag}} = \frac{\partial \Omega_{arag}}{\partial S}\Delta S + \frac{\partial \Omega_{arag}}{\partial TA}\Delta TA^S + \frac{\partial \Omega_{arag}}{\partial DIC}\Delta DIC^S. \quad (6)$$

ΔnTA and ΔnDIC are the salinity normalized deviations from the annual means of TA and DIC during the study period. ΔTA^S and ΔDIC^S are deviations from the annual means due to freshwater input, and ΔFS_{pH} and $\Delta FS_{\Omega_{arag}}$ are the total contributions of freshwater input to ΔpH and $\Delta\Omega_{arag}$, respectively (Hauri et al., 2013).

ΔpH in Hinase was primarily controlled~~contributed to~~ by ∂pH/∂T * ΔT, i.e., pH was enhanced by warmer temperature in summer and autumn and is lowered by cooler temperature in winter and spring (Fig. 14(a)). Contribution of ∂ pH/ ∂ DIC * ΔDIC, resulting from biological production, was also dominant but the phase of ∂ pH/ ∂ DIC * ΔDIC was 4-5 months different from that of ∂ pH/ ∂ T * ΔT. The two terms partly cancelled ~~out~~ each other out and formed ΔpH. ΔpH in Shizugawa, on the other hand, was primarily controlled ~~contributed to~~ by ∂ pH/ ∂ DIC * ΔDIC, and the contribution of ∂ pH/ ∂ DIC * ΔDIC was largely cancelled out by that of ∂pH/∂T * ΔT which is out of phase in most of the months (Fig. 14(b)). As a result, ΔpH was relatively small in Shizugawa.

$\Delta\Omega_{arag}$ in Hinase and Shizugawa were primarily ~~contributed to~~controlled by ∂pH/∂DIC* ΔnDIC and $\partial\Omega_{arag}$/∂DIC * ΔnDIC, that is, pH and Ω_{arag} were enhanced by lower DIC concentration in winter and spring and lowered by higher DIC concentration in summer and autumn (Fig. 14(c)-(d)). The difference between ΔpH and $\Delta\Omega_{arag}$ is that ΔpH was mainly ~~contributed to~~controlled by temperature and DIC changes while $\Delta\Omega_{arag}$ was primarily controlled by DIC and TA changes. The phases of ∂ pH/ ∂ TA* ΔnTA and ∂ Ω_{arag}/ ∂ TA* ΔnTA were almost opposite in the study period, and therefore, contributed to ΔpH and $\Delta\Omega_{arag}$ differently between Hinase and Shizugawa. The monthly-mean contributions of ΔFS_{pH} and $\Delta FS_{\Omega_{arag}}$ to ΔpH and Δ Ω_{arag} were minor.

4 Discussion

4.1 Future projection

The projected results for physical and biogeochemical parameters in the 2090s differed markedly between Hinase and

Shizugawa, and the RCP scenarios (RCP 2.6 vs. 8.5) (Figs. 15 and 16).

In Hinase, the projected rise in water temperature for the rest of this century was slight (Fig. 15 (a)), so DO concentrations will not change significantly (Fig. 15 (c)). Similarly, salinity will not change by the end of this century, leading to no significant change in TA (Fig. 15 (b), (d)). Therefore, the significant decrease in pH and Ω_{arag} values from the present to the 2090s, especially with the RCP 8.5 scenario, is likely caused by the large increase in DIC resulting from the increased atmospheric CO_2 concentrations towards the end of the century (Fig. 15 (e)). The projected results show that larvae of Pacific oysters (*C. gigas*) may experience a critical Ω_{arag} value year-round with the RCP 8.5 scenario (Fig. 15 (g)). This severe condition could be alleviated if anthropogenic CO_2 emissions are cut sufficiently in accordance with the Paris Agreement (RCP 2.6 scenario). The projected results also imply no severe impact of deoxygenation on the growth of Japanese oysters, neither now nor in the 2090s, at least at 1-m depth.

In Shizugawa, water temperatures are predicted to rise by the 2090s (Fig. 16 (a)), substantially decreasing DO concentrations (Fig. 16 (c)). Although salinity and TA values will not change from the present to the 2090s with any RCP scenario (Fig. 16 (b), (d)), DIC will increase significantly (Fig. 16 (e)). Therefore, similar to Hinase, Ω_{arag} value is predicted to decrease markedly towards the 2090s (Fig. 16 (g)), mainly because of the increase in DIC values. In Shizugawa, no severe conditions for Japanese oysters are predicted with regard to DO concentrations, but Ω_{arag} values will be below the threshold (< 1.5) except in summer, unless anthropogenic CO_2 is reduced sufficiently.

4.2 C~~Projected~~ ombined impacts of coastal warming, acidification and deoxygenation

Because estimation of the timing of start and end dates of Pacific oyster (*C. gigas*) spawning is dependent on water temperature, the timing may be altered by future coastal warming. After confirming that the simulated timing of start and end dates is consistent with the observation-based estimated timing for the present, as described in 3.2, we projected the timing for the future.

Our model results imply that in Hinase the start date will be earlier in the 2090s than at present, by two weeks with the RCP 2.6 scenario and by almost one month with the RCP 8.5 scenario, and the end date will be later by around 20 days with the RCP 8.5 scenario (Table 2; Fig. 15). In Shizugawa, the end date will be 10 days later than at present in the 2090s with the RCP 2.6 scenario and more than one month later with the RCP 8.5 scenario (Table 2; Fig. 16). With the RCP 2.6 scenario, the start date is projected to be 10 days earlier in the 2090s than at present. With the RCP 8.5 scenario, the water temperature is projected to be above 10°C year-round in the 2090s; therefore, we could not estimate the start date based on Oizumi et al. (1971).

Coastal warming and acidification may have synergistic impacts on Pacific oyster larvae. As mentioned above, coastal warming will lengthen the spawning period, which is the life stage most vulnerable to acidification. Therefore, Pacific oyster larvae may suffer from acidification more ~~seriously~~ severely and over a longer period. Our model results imply that the number of days on which Ω_{arag} values are below the threshold of acidification for Pacific oyster larvae (1.5) in Hinase will increase

from 0 days at present and with the RCP 2.6 scenario and to 204 days with the RCP 8.5 scenario in the 2090s (~~Table 3;~~ Fig. 15). With the RCP 8.5 scenario, 17 of the 204 days are during the spawning period. In Shizugawa, the number of days on which Ω_{arag} values are below 1.5 will increase from 0 days from the present and with the RCP 2.6 scenario to 244 days with the RCP 8.5 scenario in the 2090s (~~Table 3;~~ Fig. 16).

However, because of the reasons mentioned in 2.4, the model underestimated the observed short-term fluctuation of Ω_{arag} (Fig. 13). Therefore, the number of days on which Ω_{arag} values are below 1.5 is also considered to be underestimated. Assuming that the observed short-term fluctuations of Ω_{arag} at present are maintained in the future, the above simulated or projected number of days are increased from 0 to 3 days for the~~at~~ present, from 0 to 5 days with the RCP 2.6 scenario, and from 204 to 256 days with the RCP 8.5 scenario in Hinase. In Shizugawa, the projected number of days are modified from 0 to 7 days for the~~at~~ present and with the RCP 2.6 scenario, and from 244 to 322 days with the RCP 8.5 scenario (Table 3, Fig. S1). The duration of severe conditions might be 2 weeks longer, considering that 2–4 weeks are required for Pacific oyster larvae to settle after birth (*e.g.*, Chanley and Dinamani, 1980; Tachi et al., 2013). The prolonged spawning period may shorten the oyster shipping period and lower their quality (Akashige and Fushimi, 1992), potentially damaging the oyster-processing industry.

Compared to the combined impacts of coastal warming and acidification, our model results indicate that the impact of deoxygenation on Pacific oysters will be less severe, at least in surface waters. The model results reveal that the number of days on which DO concentrations are below the optimal range for Pacific oyster growth (< 203 μmol kg^{-1}) will increase in Hinase from 1 day at present to 14 and 38 days in the 2090s with the RCP 2.6 and 8.5 scenarios, respectively, and 0 days in Shizugawa at present and in the 2090s (Table 3). Similar to Ω_{arag}, however, the number of days on which DO concentrations are below 203 μmol kg^{-1} is considered to be even greater~~more~~ if the observed significant short-term fluctuation (Fig. 10) is assumed. However, we could not take the short-term fluctuation into account because of the lack of ~~the~~ continuous ~~short term~~ DO observations (Fig. 11)~~ed short-term fluctuation~~.

4.3 Thresholds for impacts of ocean acidification on Pacific oysters in Japan coasts

In this study, impacts of ocean acidification on Pacific oysters (*C. gigas*) were evaluated by using the threshold of Ω_{arag}=1.5 (Waldbusser et al., 2015). On the other hand, as mentioned in 3.1, by microscopic examination we did not observe any morphological abnormalities in the larvae (Fig. 7), and therefore, we did not find any anecdotal evidence of impacts of ocean acidification on Pacific oyster larvae in this study. This is different from the situation in the West Coast of the USA where oyster farms have already been reported to be impacted by low-pH, low-Ω_{arag} seawater (e.g. Barton et al., 2012), as mentioned in Section 1. We need to clarify the discrepancy between the scientific findings and the fact that no specific impacts of ocean acidification on Pacific oyster larvae have so far been detected in the study sites, even they occasionally experience the critical level of ocean acidification proposed by a previous study (Ω_{arag} < 1.5; Waldbusser et al., 2015).

It is possible that we failed to collect abnormal larvae samples for the reason that the abnormal larvae died before our samples were taken, although it is unlikely that there were many such abnormal larvae present. If so, the plankton nets would have been able to collect sufficient numbers of them to be detected under microscopic examination.

Rearing experiments of Waldbusser et al. (2015) were performed in Oregon, USA, where Pacific oysters are not native, while they are native in both the Hinase Area and Shizugawa Bay. Therefore, it is possible that the Pacific oysters in Hinase and Shizugawa have already partly adapted to local environmental changes, including lower pH and Ω_{arag} conditions caused by riverine discharge of freshwater and organic matter. To verify this, we might need further examination including new rearing experiments for native Pacific oyster species in Japan coasts.

Previous studies also suggest that oyster larvae have decreased swimming ability and sink as salinity decreases (e.g. Dekshennieks et al., 1996). Therefore, it is possible that the Pacific oyster larvae did not remain in low-salinity waters, and consequently could escape from the lower pH and Ω_{arag} conditions. These issues should be taken into consideration in future works, although not in this study, and therefore, the impacts of ocean acidification on Pacific oysters may have been overestimated in this sense. Also, considering that our current model underestimated observed sudden decreases in salinity as mentioned in 3.2, more realistic input data of freshwater from rainfall and riverine water would be necessary for better model performance.

5 Conclusion ~~and Remark~~s

Impacts of ongoing coastal warming, acidification, and deoxygenation on Pacific oysters in Japan coasts have not been clarified before. This study aimed to assess the current and project the future impacts, through continuous monitoring, microscopic examination, and numerical modeling in two representative oyster farming regions in Japan, the Hinase Area and Shizugawa Bay. This study first elucidated that oyster-farming sites in Hinase have experienced critical levels of acidification, although Pacific oyster larvae do not seem to have been affected. It may therefore be necessary to revisit the acidification threshold for Pacific oysters farmed in Japan coasts.

Our future projections imply that unless CO_2 emissions are reduced in accordance with the Paris Agreement (RCP 2.6 scenario), oyster farming at the study sites may be seriously affected by coastal warming and acidification by the end of this century. The greatest impact will be on larvae, as a result of longer exposure to more acidified waters. A prolonged spawning period may harm oyster processing by shortening the shipping period and reducing oyster quality. Therefore, to minimize impacts on Pacific oyster farming, in addition to mitigation measures, local adaptation measures—such as regulation of freshwater and organic matter inflow from rivers and changes in oyster-farming practices—may be required.

Climate-change-driven extreme events will cause more frequent and intense heavy rainfall; subsequent river inflow of freshwater and organic matter to coasts may further reduce pH and Ω_{arag} in oyster farms. To plan how to minimize the adverse impacts of coastal warming and acidification, coupled physical-biogeochemical models with higher spatiotemporal resolution are needed to simulate river-inflow processes and daily fluctuations in biogeochemical parameters.

Author contributions

TT launched the research project; AD and SO performed the measurements; MW analyzed the samples; LPCB and RH performed the model~~l~~ing; MF, RH, and TO analyzed the data; RH and MF wrote the manuscript draft; LPCB, TO, AD, SO, MW, and TT reviewed and edited the manuscript.

Competing interests

The authors declare that they have no conflict of interest.

Acknowledgments.

We thank Wakako Takeya and Jen-Han Yang for support, and Miho Ishizu and anonymous reviewers for their useful comments. This study was supported by the Nippon Foundation Ocean Acidification Adaptation Project (OAAP), ~~the Integrated Research Program for Advancing Climate Models (TOUGOU; Grant Numbers JPMXD0717935498 and JPMXD0717935715), and~~ Theme 4 of the Advanced Studies of Climate Change Projection (SENTAN Program)~~;~~ Grant Number JPMXD0722678534~~)~~ supported by~~,~~ the Ministry of Education, Culture, Sports, Science, and Technology (MEXT), ~~of~~ Japan, and the Hokkaido University Functional Enhancement Project. This study used the Future Ocean Regional Projection dataset, which was produced by the Japan Agency for Marine-Science and Technology (JAMSTEC) under the SI-CAT project (Grant Number JPMXD0715667163) of the Ministry of Education, Culture, Sports, Science and Technology of Japan. FORPJPN02 version 2 was provided by JAMSTEC and was collected and provided under the Data Integration and Analysis System (DIAS), which was developed and operated by a project supported by the Ministry of Education, Culture, Sports, Science and Technology, Japan. We used a coupled physical-biogeochemical model that was constructed under the framework of the Study of Biological Effects of Acidification and Hypoxia (BEACH) of the Environment Research and Technology Development Fund (Grant Number JPMEERF20202007) of the Environmental Restoration and Conservation Agency of Japan.

References

Abo, K., and Yamamoto, T.: Oligotrophication and its measures in the Seto Inland Sea, Japan, Bulletin of Japan Fisheries Research and Education Agency, 49, 21-26, 2019.

Akashige, S., and Fushimi, T.: Growth, survival, and glycogen content of triploid Pacific oyster *Crassostrea gigas* in the waters of Hiroshima, Japan, Nippon Suisan Gakkaishi, 58(6), 1063-1071, 1992.

Ando, H., Maki, H., Kashiwagi, N., and Ishii, Y.: Long-term change in the status of water pollution in Tokyo Bay: recent trend of increasing bottom-water dissolved oxygen concentrations, J. Oceanogr., 77, 843-858, doi:10.1007/s10872-021-00612-7, 2021.

Anthony, K. R., Kline, D. I., Diaz-Pulido, G., Dove, S., and Hoegh-Guldberg, O.: Ocean acidification causes bleaching and productivity loss in Proceedings of the National Academy of Sciences, 105(45), 17442-17446, 2008.

The Association for Environmental Conservation of the Seto Inland Sea: The Seto Inland Sea: The largest enclosed coastal sea in Japan, available at: https://www.seto.or.jp/upload/publish/setonaikai_heisaseikaiiki.pdf, last access: 31 October 2022.

Aumont, O.: PISCES biogeochemical model, 36pp., 2005, available at: https://data-croco.ifremer.fr/papers/manuel_pisces.pdf, last access: 5 May 2023.

Aumont, O., Maier-Reimer, E., Blain, S., and Monfray, P.: An ecosystem model of the global ocean including Fe, Si, P Colimitations. Glob. Biogeochem. Cycles, 17(2), 1-26, 2003.

Barton, A., Hales, B., Waldbusser, G., Langdon, C., and Feely, R. A.: The Pacific oyster, *Crassostrea gigas*, shows negative correlation to naturally elevated carbon dioxide levels: Implications for near-term ocean acidification effects. Limnol. Oceanography, 57(3), 698–710, doi:10.4319/lo.2012.57.3.0698, 2012.

Bates, N. R., Astor, Y. M., Church, M. J., Currie, K., Dore, J. E., González-Dávila, M., Lorenzoni, L., Muller-Karger, F. Olafsson, J., and Santana-Casiano., J. M.: A time-series view of changing ocean chemistry due to ocean uptake of anthropogenic CO_2 and ocean acidification. Oceanography, 27(1), 126–141, doi: 10.5670/oceanog.2014.16, 2014.

Bernardo, L. P. C., Fujii, K., and Ono, T.: Development of a high-resolution marine ecosystem model for predicting the combined impacts of ocean acidification and deoxygenation, Front. Mar. Sci., in revision, 2023.~~Prediction of combined effects of ocean acidification and anoxia using a high-resolution marine ecosystem model, Proceedings of the 2021 Japan Society of Fisheries Oceanography Conference, 44, November 21, 2021, Nagasaki, Japan, 2021.~~

Booth, J. A. T., McPhee-Shaw, E. E., Chua, P., Kingsley, E., Denny, M., Phillips, R., Bograd, S. J., Zeidberg, L. D. and Gilly, W. F.: Natural intrusions of hypoxic, low pH water into nearshore marine environments on the California coast, Cont. Shelf Res., 45, 108-115, doi:10.1016/j.csr.2012.06.009, 2012.

Breitburg, D., Levin, L. A., Oschlies, A., Grégoire, M., Chavez, F. P., Conley, D. J., Garçon, V., Gilbert, D., Gutiérrez, D., Isensee, K., Jacinto, G. S., Limburg, K. E., Montes, I., Naqvi, S. W. A., Pitcher, G. C., Rabalais, N. N., Roman, M. R., Rose, K. A., Seibel, B. A., Telszewski, M., Yasuhara, M., and Zhang, J.: Declining oxygen in the global ocean and coastal waters, Science, 359, 6371, doi:10.1126/science.aam7240, 2018.

Chanley, T. P., and Dinamani, P.: Comparative descriptions of some oyster larvae from New Zealand and Chile, and a description of a new genus of oyster, New Zealand Journal of Marine & Freshwater Research, 14(2): 103-120, 1980.

Da Silva, A., Young, A. C., and Levitus, S.: Atlas of Surface Marine Data 1994. Vol. 1: Algorithms and Procedures, NOAA Atlas NESDIS 6, U.S. Department of Commerce, Washington, DC, USA, 74pp, 1994.

Dekshennieks, M. M., Hofmann, E. E., Klink, J. M., and Powell, E. N.: Modeling the vertical distribution of oyster larvae in response to environmental conditions, Mar. Ecol. Prog. Ser., 136, 97-110, 1996.

DePasquale, E., Baumann, H., and Gobler, C. J.. Vulnerability of early life stage Northwest Atlantic forage fish to ocean acidification and low oxygen, Mar. Ecol. Prog. Ser., 523, 145–156, doi:10.3354/meps11142, 2015.

DeJong, H. B., Dunbar, R. B., Mucciarone, D., and Koweek, D. A.: Carbonate saturation state of surface waters in the Ross Sea and Southern Ocean: controls and implications for the onset of aragonite undersaturation, Biogeosci., 12, 6881-6896, 2015.

Dickson, A. G.: Standard potential of the reaction: $AgCl(s) + \frac{1}{2}H_2(g) = Ag(s) + HCl(aq)$, and the standard acidity constant of the ion HSO_4^- in synthetic sea water from 273.15 to 318.15 K, J. Chem. Thermodynamics, 22, 113–127, 1990.

Doney, S. C., Busch, D. S., Cooley, S. R., and Kroeker, K. J.: The impacts of ocean acidification on marine ecosystems and reliant human, Annu. Rev. Environ. And Resour., 45(1), 83-112, 2020.

Durland, E., Waldbusser, G., and Langdon, C.: Comparison of larval development in domesticated and naturalized stocks of Pacific oyster *Crassostrea gigas* exposed to high pCO_2 conditions, Mar. Ecol. Prog. Ser., 621, 107-125, 2019.

Egbert, G. D., and Erofeeva S. Y.: Efficient inverse modeling of barotropic ocean tides, J. Atmos. Oceanic Technol., 19(2), 183-204, 2002.

Fisheries Agency: Guidelines for the introduction of technologies to improve the environment of bivalve fishing grounds, 2013, available at: https://www.jfa.maff.go.jp/j/kenkyu/pdf/pdf/3-3.pdf, last access: 1 February 2022.

Fujii, M., Takao, S., Yamaka, T., Akamatsu, T., Fujita, Y., Wakita, M., Yamamoto, A., and Ono, T.: Continuous monitoring and future projection of ocean warming, acidification, and deoxygenation on the subarctic coast of Hokkaido, Japan, Front. Mar. Sci., 8, 590020, 2021.

Garcia, H. E., Locarnini, R. A., Boyer, T. P., Antonov, J. I., Baranova, O. K., M. M. Zweng, and Johnson, D. R.: World Ocean Atlas 2009, Volume 3: Dissolved Oxygen, Apparent Oxygen Utilization, and Oxygen Saturation. S, edited by: Levitus, S., NOAA Atlas NESDIS 70, U.S. Government Printing Office, Washington, D.C., 344pp, 2010a.

Garcia, H. E., Locarnini, R. A., Boyer, T. P., Antonov, J. I., Zweng, M. M., Baranova, O. K., and Johnson, D. R.: World Ocean Atlas 2009, Volume 4: Nutrients (phosphate, nitrate, silicate), edited by: Levitus, S., NOAA Atlas NESDIS 71, U.S. Government Printing Office, Washington, D.C., 398pp, 2010b.

Gazeau, F., Quiblier, C., Jansen, J. M., Gattuso, J.-P., Middelburg, J. J., and Heip, C. H.: Impact of elevated CO_2 on shellfish calcification, Geophys. Res. Lett., 34(7), L07603, 2007.

General Bathymetric Chart of the Oceans (GEBCO) website: Gridded Bathymetry Data, available at: https://www.gebco.net/data_and_products/gridded_bathymetry_data/, last access: 14 October 2022.

Gimenez, I., Waldbusser, G. G., and Hales, B.: Ocean acidification stress index for shellfish (OASIS): Linking Pacific oyster larval survival and exposure to variable carbonate chemistry regimes. Elementa: Science of the Anthropocene, 6, 51, 2018.

Gobler, C. J., and Baumann, H.: Hypoxia and acidification in ocean ecosystems: coupled dymanics and effects on marine life, Biol. Lett., 12, 20150976, doi:10.1098/rsbl.2015.0976, 2016.

Guinotte, J. M., and Fabry V. J.: Ocean acidification and its potential effects on marine ecosystems, Annals of the New York Academy of Sciences, 1134(1), 320-342, 2008.

Hamanoue, R.: Assessment of impacts of ocean acidification on Pacific oyster (*Crassostrea gigas*): A case study in the Hinase Area, Okayama Prefecture and Shizugawa Bay, Miyagi Prefecture, Master's Thesis, Graduate School of Environmental Science, Hokkaido University, 88pp, 2022 (in Japanese).

Hauri, C., Gruber, N., Vogt, M., Doney, S. C., Feely, R. A., Lachkar, Z., Leinweber, A., McDonnell, A. M. P., Munnich, M., and Plattner, G.-K.: Spatiotemporal variability and long-term trends of ocean acidification in the California Current System, Biogeosci., 10, 193-216, 2013.

Helm K. P., Bindoff , N. L., Church, J. A.: Observed decreases in oxygen content of the global ocean, Geophys. Res. Lett., 38, L23602, doi:10.1029/2011GL049513, 2011.

Hochachka, P. W., Coupled glucose and amino acid catabolism in bivalve mollusks, in: Living without oxygen: closed and open systems in hypoxia tolerance, Harvard University Press, Cambridge, 25-41, 1980.

Horii, H., Tanaka, H., Watanabe, K., and Shuto, N.: In-situ observations of water mass exchange in Shizugawa Bay, Proc. Coast. Eng., 41, 1091-1095, 1994. (in Japanese).

Hoshiba, Y., Hasumi, H., Itoh, S., Matsumura, Y., and Nakada, S.: Biogeochemical impacts of flooding discharge with high suspended sediment on coastal seas: a modeling study for a microtidal open bay, Sci. Rep., 11(1), 21322, 2021.

Imai, I., Yamaguchi, M., and Hori, Y.: Eutrophication and occurrences of harmful algal blooms in the Seto Inland Sea, Japan, Plankton and Benthos Research, 1, 71-84, 2006.

Intergovernmental Panel on Climate Change (IPCC): Global Warming of 1.5 °C. An IPCC Special Report on the impacts of global warming of 1.5 °C above pre-industrial levels and related global greenhouse gas emission pathways, in the context of strengthening the global response to the threat of climate change, sustainable development, and efforts to eradicate poverty, edited by: Masson-Delmotte, V., Zhai, P., Pörtner, H. -O., Roberts, D., Skea, J., Shukla, P. R., Pirani, A., Moufouma-Okia, W., Péan, C., Pidcock, R., Connors, S., Matthews, J. B. R., Chen, Y., Zhou, X., Gomis, M. I., Lonnoy, E., Maycock, T., Tignor, M., and Waterfield, T., Cambridge University Press, Cambridge, UK and New York, NY, USA, 630pp, 2018, available at: https://www.ipcc.ch/site/assets/uploads/sites/2/2019/06/SR15_Full_Report_High_Res.pdf, last access: 14 October 2022.

IPCC: IPCC Special Report on the Ocean and Cryosphere in a Changing Climate, edited by: Pörtner, H. -O., Roberts, D. C., Masson-Delmotte, V., Zhai, P., Tignor, M., Poloczanska, E., Mintenbeck, K., Alegria, A., Nicolai M., Okem, A., Petzold, J., Rama, B., and Weyer, N. M., Cambridge University Press, Cambridge, United Kingdom and New York, NY, USA, 765pp, 2019, available at: https://www.ipcc.ch/site/assets/uploads/sites/3/2019/12/SROCC_FullReport_FINAL.pdf, last access: 14 October 2022.

IPCC: Summary for Policymakers. In: Climate Change 2021: The Physical Science Basis. Contribution of Working Group I to the Sixth Assessment Report of the Intergovernmental Panel on Climate Change, edited by: Masson-Delmotte, V., Zhai, P., Pirani, A., Connors, S. L., Péan, C., Berger, S., Caud, N., Chen, Y., Goldfarb, L., Gomis, M. I., Huang, M., Leitzell, K.,

Lonnoy, E., Matthews, J. B. R., Maycock, T. K., Waterfield, T., Yelekçi, O., Yu, R., and Zhou, B., Cambridge University Press, Cambridge, United Kingdom and New York, NY, USA, 3-32, doi:10.1017/9781009157896.001, 2021.

Ito, T., Minobe, S., Long, M. C., and Deutch, C.: Upper ocean O_2 trends: 1958–2015, Geophys. Res. Lett., 44, 4214–4223, doi:10.1002/2017GL073613, 2017.

Japan Meteorological Agency website: available at: https://www.data.jma.go.jp/obd/stats/etrn/index.php, last access: 14 October 2022.

Japan Meteorological Agency website: NetCDF data (MSM, RSM) reconstructed around analysis values, available at: http://database.rish.kyoto-u.ac.jp/arch/jmadata/gpv-netcdf.html, last access: 14 October 2022.

Jiang, L.-Q., Carter, B. R., Feely, R. A., Lauvset, S. K., and Olsen, A.: Surface ocean pH and buffer capacity: past, present and future, Sci. Rep., 9, 18624, doi:.10.1038/s41598-019-55039-4, 2019.

Jullien, S., Caillaud, M., Benshila, R., Bordois, L., Cambon, G., Dumas, F., Le Gentil, S., Lemarié, F., Marchesiello, P., and Theetten, S.: Croco Tutorials Release 1.1, 2019, available at: https://data-croco.ifremer.fr/DOC/tutos-v1.1.pdf, last access: 1 November 2022.

Kessouri, F., McWilliams, J. C., Bianchi, D., Sutula, M., Renault, L., Deutsch, C., Feely, R. A., McLaughlin, K., Ho, M., Howard, E. M., Bednaršek, N., Damien, P., Molemaker, J., and Weisberg, S. B.: Coastal eutrophication drives acidification, oxygen loss, and ecosystem change in a major oceanic upwelling system, Proc. Nat. Acad. Sci., 118, e2018856118, doi: 10.1073/pnas.2018856118, 2021.

Kimura, R., Takami, H., Ono, T., Onitsuka, T., and Nojiri, Y.: Effects of elevated pCO_2 on the early development of the commercially important gastropod, Ezo abalone *Haliotis discus hannai*. Fish. Oceanogr. 20, 357–366, doi:10.1111/j.1365-2419.2011.00589.x, 2011.

Koslow, J.A., Goericke R., Lara-Lopez, A., and Watson, W.: Impact of declining intermediate-water oxygen on deep water fishes in the California Current, Mar. Ecol. Prog. Ser., 436, 207-218, doi:10.3354/meps09270, 2011.

Koslow, J. A., Miller, E. F., and McGowan, J. A.: Dramatic declines in coastal and oceanic fish communities off California, Mar. Ecol. Prog. Ser., 538, 221–227, doi:10.3354/meps11444, 2015.

Komatsu, T., Sasa, S., Montani, S., Yoshimura, C., Fujii, M., Natsuike, M., Nishimura, O., Sakamaki T., and Yanagi, T.: Studies on a coastal environment management method for an open-type bay: the case of Shizugawa Bay in Southern Sanriku Coast, Bulletin on Coastal Oceanography, 56(1), 21-29, 2018 (in Japanese with English abstract).

Kurihara, H.: Effects of CO_2-driven ocean acidification on the early developmental stages of invertebrates, Mar. Ecol. Prog. Ser., 373, 275-284, 2008.

Kurihara, H., Kato, S., and Ishimatsu, A.: Effects of increased seawater pCO_2 on early development of the oyster *Crassostrea gigas*, Aquat. Biol., 1, 91-98, 2007.

Laffoley, D., Baxter, J.M. (eds.): Ocean deoxygenation: Everyone's problem – Causes, impacts, consequences and solutions. Full report. Gland, Switzerland: IUCN. 580pp, 2019.

Lee, K., Kim, T.-W., Byrne, R. H., Millero, F. J., Feely, R. A. Liu, Y.-M., The universal ratio of boron to chlorinity for the North Pacific and North Atlantic oceans, Geochimica et Cosmochimica Acta, 74 (6), 1801-1811, 2010.

Le Quéré, C., Andrew, R. M., Friedlingstein, P., Sitch, S., Hauck, J., Pongratz, J., Pickers, P. A., Korsbakken, J. I., Peters, G. P., Canadell, J. G, Arneth, A., Arora, V. K., Barbero, L., Bastos, A., Bopp, L., Chevallier, F., Chini, L. P., Ciais, P., Doney, S. C., Gkritzalis, T., Goll, D. S., Harris, I, Haverd, V., Hoffman, F. M., Hoppema, M., Houghton, R. A., Hurtt, G., Ilyina, T., Jain, A. K., Johannessen, T., Jones, C. D., Kato, E., Keeling, R. F, Goldewijk, K. K., Landschützer, P., Lefèvre, N., Lienert, S., Liu, Z., Lombardozzi, D., Metzl, N., Munro, D. R., Nabel, J. E. M. S., Nakaoka, S., Neill, C, Olsen, A., Ono, T., Patra, P., Peregon, A., Peters, W., Peylin, P., Pfeil, B., Pierrot, D., Poulter, B., Rehder, G., Resplandy, L., Robertson, E., Rocher, M., Rödenbeck, C., Schuster, U., Schwinger, J., Séférian, R., Skjelvan, I., Steinhoff, T., Sutton, A., Tans, P. P., Tian, H., Tilbrook, B., Tubiello, F. N., van der Laan-Luijkx, I. T., van der Werf, G. R., Viovy, N., Walker, A. P., Wiltshire, A. J., Wright, R., Zaehle, S., and Zheng, B.: Global Carbon Budget 2018. Earth System Science Data, 10(4), 2141-2194, 2018.

Levitus, S., Antonov, J. I., Boyer, T. P., Locarnini, R. A., Garcia, H. E., and Mishonov, A. V.: Global Ocean Heat Content 1955-2008 in light of recently revealed instrumentation problems, Geophy. Res. Lett., 36(7), L07608, 2009.

Lewis, E., and Wallace, D., and Allison, L. J.: Program developed for CO_2 system calculations, ORNL/CDIAC-105, Oak Ridge Natl. Lab, 33pp, doi:10.2172/639712, 1998.

Limburg, K. E., Breitburg, D., Swaney, D. P., and Jacinto, G.: Ocean deoxygenation: A primer, One Earth, 2, 24-29, doi: 10.1016/j.oneear.2020.01.001, 2020.

Lueker, T. J., Dickson, A. G., and Keeling, C. D.: Ocean pCO_2 calculated from dissolved inorganic carbon, alkalinity, and equations for K1 and K2: validation based on laboratory measurements of CO_2 in gas and seawater at equilibrium, Mar. Chem., 70, 105–119, doi:10.1016/s0304-4203(00)00022-0, 2000.

Melzner, F., Thomsen, J., Koeve, W., Oschilies, A., Gutowska, M. A., Bange, H. W., Hansen, H., P., and Körtzinger, A.: Future ocean acidification will be amplified by hypoxia in coastal habitats, Mar. Biol., 160, 1875-1888, doi:10.1007/s00227-012-1954-1, 2013.

Ministry of Agriculture, Forestry and Fisheries website: available at: https://www.maff.go.jp/j/tokei/kouhyou/kaimen_gyosei/, last access: 14 October 2022.

Ministry of the Environment: Guide book of environments in enclosed sea areas (88 areas), Ministry of Environment of Japan, Tokyo, 407, 2010. (in Japanese)

Ministry of the Environment website: available at: https://water-pub.env.go.jp/water-pub/mizu-site/mizu/kousui/dataMap.asp, last access: 14 October 2022.

Morse, J. W., Mucci, A., and Millero, F. J.: The solubility of calcite and aragonite in seawater of 35%, Geochimica et Cosmochimica Acta, 44(1), 85-94, 1980.

Ning, X., Lin, C., Su, J., Liu, C., Hao, Q., and Le, F.: Long-term changes of dissolved oxygen, hypoxia, and the responses of the ecosystems in the East China Sea from 1975 to 1995, J. Oceanogr., 67, 59-75, doi:10.1007/s10872-011-0006-7, 2011.

Nishikawa, S., Wakamatsu, T., Ishizaki, H., Sakamoto, K., Tanaka, Y., Tsujino, H., Yamanaka, G., Kamachi, M., and Ishikawa, Y.: Development of high-resolution future ocean regional projection datasets for coastal applications in Japan, Progress in Earth and Planetary Science, 8(1), 2021.

Nomura, M., Chiba, N., Xu, K.-Q., and Sudo, R.: The formation of anoxic water mass in Shizugawa Bay, The Oceanographic Society of Japan, 2, 33, 203-210, 1996. (in Japanese with English abstract)

Oizumi S., Ito, S., Koganezawa, A., Sakai, S., Sato, R., and Kanno, H.: Techniques of oyster culture, in: Aquaculture in. shallow seas: progress in shallow sea culture (Revised edition), edited by: Imai T., Koseisha Koseikaku, Tokyo, 153-189, 1971 (in Japanese).

Onitsuka, T., Kimura, R., Ono, T., Takami, H., and Y. Nojiri, Y.: Effects of ocean acidification on the early developmental stages of the horned turban, *Turbo cornutus*, Mar. Biol., 161(5), 1127-1138, 2014.

Onitsuka, T., Takami, H., Muraoka, D., Matsumoto, Y., Nakatsubo, A., Kimura, R., Ono, T., and Nojiri, Y.: Effects of ocean acidification with pCO_2 diurnal fluctuations on survival and larval shell formation of ezo abalone, *Haliotis discus hannai*. Marine Environmental Research, 134, 28-36, 2018.

Ono, T.: Long-term trends of oxygen concentration in the waters in bank and shelves of the Southern Japan Sea, J. Oceanogr., 77, 659-684, doi: 10.1007/s10872-021-00599-1, 2021.

Orr, J. C., Fabry, V. J., Aumont, O., Bopp, L., Doney, S. C., Feely, R. A., Gnanadesikan, A., Gruber, N., Ishida, A., Joos, F., Key, R. M., Lindsay, K., Slater, R. D., Totterdell, I. J., Weirig, M.-F., Yamanaka, Y., and Yool, A.: Anthropogenic ocean acidification over the twenty-first century and Nature, 437(7059), 681-686, doi:10.1038/nature04095, 2005.

Oschlies, A., Brandt, P., Stramma, L., Schmidtko, S.: Drivers and mechanisms of ocean deoxygenation, Nat. Geosci., 11, 467-473, doi:10.1038/s41561-018-0152-2, 2018.

Papalexiou, S. M., and Montanari, A.: Global and regional increase of precipitation extremes under global warming, Water Resources Research, 55, 4901-4914, 2019.

Perez, F. F., Fraga, F.: Association constant of fluoride and hydrogen ions in seawater, Mar. Chem., 21(2), 161-168, 1987.

Pierrot, D., Lewis, E., and Wallace, D. W. R.: MS Excel program developed for CO_2 system calculations. ORNL/CDIAC-105a. Oak Ridge, TN: Carbon Dioxide Information Analysis Center, Oak Ridge National Laboratory, doi:10.3334/CDIAC/otg.CO2SYS_XLS_CDIAC105a, 2006.

Rabalais, N. N., Díaz, R. J., Levin, L. A., Turner, R. E., Gilbert, D., and Zhang, J.: Dynamics and distribution of natural and human-caused hypoxia, Biogeosci., 7, 585–619, doi:10.5194/bg-7-585-2010, 2010.

Sasano, D., Takatani, Y., Kosugi, N., Nakano, T., Midorikawa, T., and Ishii, M.: Multidecadal trends of oxygen and their controlling factors in the western North Pacific, Glob. Biogeochem. Cycles., 29, 935-956, doi:10.1002/2014GB005065, 2015.

Sasano, D., Takatani, Y., Kosugi, N., Nakano, T., Midorikawa, T., and Ishii, M.: Decline and bidecadal oscillations of dissolved oxygen in the Oyashio region and their propagation to the western North Pacific, Glob. Biogeochem. Cycles, 32, 909-931, doi:10.1029/2017GB005876, 2018.

Schmidtko, S., Stramma, L., and Visbeck, M.: Decline in global oceanic oxygen content during the past five decades, Nature, 542, 335-339, doi:10.1038/nature21399, 2017.

Stramma, L., Oschlies, A., and Schmidtko, S.: Mismatch between observed and modeled trends in dissolved upper-ocean oxygen over the last 50 yr, Biogeosci., 9, 4045-4057, doi:10.5194/bg-9-4045-2012, 2012.

Stramma, L, Prince, E. D., Schmidtko, S., Luo, J., Hooliham, J. P., Visbeck, M., Wallace, D. W. R., Brandt, P., Kortzinger, A.: Expansion of oxygen minimum zones may reduce available habitat for tropical pelagic fishes, Nat. Clim. Change, 2, 33-37, doi: 10.1038/ NCLIMATE1304, 2011.

Stramma, L., Schmidtko, S., Bograd, S. J., Ono, T., Ross, T., Sasano, D., and Whitney, F. A.: Trends and decadal oscillations of oxygen and nutrients at 50 to 300 m depth in the equatorial and North Pacific, Biogeosci, 17, 813-831, doi: 10.5194/bg-17-813-2020, 2020.

Stramma, L., Schmidtko, S., Levin, L. A., and Johnson, G. C.: Ocean oxygen minima expansions and their biological impacts, Deep-Sea Res. Part I, 57, 587-595, doi:10.1016/j.dsr.2010.01.005, 2010.

Suzuki, M., Nakatani, Y., and Koga, Y.: Evaluating the effects of operations to increase nitrogen discharge from sewage treatment plants on concentrations of organic matter and nutrients in surface water at Harima-nada in the Seto Inland Sea, Journal of Japan Society of Water Environment, 43(2), 43-53, 2020 (in Japanese with English abstract).

Tachi, H., Hata, N., Saitou, Y., and Iwao, T.: An attempt to collect the natural spat of Japanese oyster *Crassostrea gigas* in the coast of Toba-Shima, Mie prefecture, Bull. Mie Pref. Fish. Res. Inst., 22, 17-24, 2013 (in Japanese).

Taylor, K. E., Stouffer, R. J., and Meehl, G. A.: An overview of CMIP5 and the experiment design, Bull. Am. Meteorol. Soc., 93(4), 485-498, doi:10.1175/BAMS-D-11-00094.1, 2012.

Tsujino, H., Nakano, H., Sakamoto, K., Urakawa, S., Hirabara, M., Ishizaki, H., and Yamanaka, G.: Reference manual for the Meteorological Research Institute Community Ocean Model version 4 (MRI.COMv4). Technical Reports of the MRI, 80, doi:10.11483/mritechrepo.80, 2017.

Van Vuuren, D. P., Edmonds, J., Kainuma, M., Riahi, K., Thomson, A., Hibbard, K., Hurtt, G. C., Kram, T., Krey, V., Lamarque, J.-F., Masui, T, Meinshausen, M., Nakicenovic, N., Smith, S. J., and Rose, S. K.: The representative concentration pathways: an overview, Climatic Change, 109, 5-31, 2011.

Wada, S., Ishii, M., Kosugi, N., Sasano, D., Matsushita, W., Omori, Y., and Hama, T.: Seasonal dynamics of seawater CO_2 system at a coastal site near the southern tip of Izu Peninsula, Japan, J. Oceanogr., 76, 227-242, 2020.

Wakita, M., Nagano, A., Fujiki, T., and Watanabe, S.: Slow acidification of the winter mixed layer in the subarctic western North Pacific, J. Geophys. Res. Oceans, 122(8), 6923-6935, 2017.

Wakita, M., Sasaki, K., Nagano, A., Abe, H., Tanaka, T., Nagano, K., Sugie, K., Kaneko, H., Kimoto, K., Okunishi, T., Takada, M., Yoshino, J., and Watanabe, S.: Rapid reduction of pH and $CaCO_3$ saturation state in the Tsugaru Strait by the intensified Tsugaru warm current during 2012–2019, Geophys. Res. Lett., 48(10), GL091332, 2021.

Waldbusser, G. G., Hales, B., Langdon, C. J., Haley, B. A., Schrader, P., Brunner, E. L., Gray, M. W., Miller, C. A., and Gimenez, I.: Saturation-state sensitivity of marine bivalve larvae to ocean acidification, Nat. Clim. Change, *5*(3), 273-280, 2015.

Wallace, R. B., Baumann, H., Grear, J. S., Aller, R. C., and Gobler, C. J.: Coastal ocean acidification: The other eutrophication problem, Estuarine, Coastal and Shelf Science, 148, 1-13, 2014.

Watanabe, S., Hajima, T., Sudo, K., Nagashima, T., Takemura, T., Okajima, H., Nozawa, T., Kawase, H., Abe, M., Yokohata, T., Ise, T., Sato, H., Kato, E., Takata, K., Emori, S., and Kawamiya, M.: MIROC-ESM 2010: model description and basic results of CMIP5-20C3M experiments, Geosci. Model Dev., 4(4), 845-872, doi:10.5194/gmd-4-845-2011, 2011.

Watanabe, Y. W., Li, B. F., Yamasaki, R., Yunoki, S., Imai, K., Hosoda, S., and Nakano, Y.: Spatiotemporal changes of ocean carbon species in the western North Pacific using parameterization technique, J. Oceanogr., 76(2), 155-167, 2020.

Wei, Q., Yao, Q., Wang, B., Xue, L., Fu, M., Sun, J., Liu, X., and Yu, Z.: Deoxygenation and its controls in a semienclosed shelf ecosystem, northern Yellow Sea, J. Geophys., Res., 124, 9004-9019, doi:10.1029/2019JC015399, 2019.

Xiong, T., Wei, Q., Zhai, W., Li, C., Wang, S., Zhang, Y., Liu, S., and Yu, S.: Comparing subsurface seasonal deoxygenation and acidification in the Yellow Sea and northern East China Sea along the north-to-south latitude gradient, Front. Mar. Sci., 7, 686, doi: 10.3389/fmars.2020.00686, 2020.

Yamaka, T.: Assessment and future projection of variational characteristics of global warming and ocean acidification proxies in Oshoro Bay, Hokkaido. Master's thesis. Graduate School of Environmental Science, Hokkaido University, 74pp, 2019 (in Japanese).

Yamamoto, T., Orimoto, K., Asaoka, S., Yamamoto, H., and Onodera, S.: A Conflict between the legacy of eutrophication and cultural oligotrophication in Hiroshima Bay, Oceans, 2, 546-565, doi:10.3390/oceans2030031, 2021.

Yamamoto-Kawai, M., Kawamura, N., Ono, T., Kosugi, N., Kubo, A., Ishii, M., and Kanda, J.: Calcium carbonate saturation and ocean acidification J. Oceanogr., 71(4), 427-439, 2015.

Yara, Y., Oshima, K., Fujii, M., Yamano, H., Yamanaka, Y., and Okada, N.: Projection and uncertainty of the poleward range expansion of coral habitats in response to sea surface temperature warming: A multiple climate model study, Galaxea, Journal of Coral Reef Studies, 13(1). Pp. 11-20, 11-20, 2011.

Yoshino, J., Arakawa, S., Toyoda, M., and Kobayashi, T.: Inter-scenario comparison of warming effects on typhoon intensity using a high-resolution typhoon model, Doboku Gakkai Ronbunshuu, B2 (Coastal Engineering), 71(2), I_1519-I_1524, 2015 (in Japanese).

Zhang, J., Gilbert, D., Gooday, A. J., Naqvi, S. W. A., Middelburg, J. J., Scranton, M., Ekau, W., Pena, A., Dewitte, B., Oguz, T., Monteiro, P. M. S., Urban, E., Rabalais, N. N., Ittekkot, V., Kemp, W. M.: Natural and human-induced hypoxia and consequences for coastal areas: synthesis and future development, Biogeosci. 7, 1443-1467, doi:10.5194/bg-7-1443-2010, 2010.

Table 1: Boundary conditions for the coupled physical-biogeochemical model used in this study. For boundary conditions of dissolved oxygen (DO) and nutrients, the present replicate values were given for the 2090s.

Parameter	Dataset	Source
Bathymetry	The 15 arc-second General Bathymetric Chart of the Oceans (GEBCO) 2021 dataset	GEBCO website (https://www.gebco.net/data_and_products/gridded_bathymetry_data/)
Tide	TPXO Global Tidal Models (TPXO7.0)	Egbert and Erofeeva (2002)
Ocean physics (water temperature, salinity, current velocity, water level)	Future Ocean Regional Projection (FORP)-JPN02	Tsujino et al. (2017) Nishikawa et al. (2021)
Atmospheric forcing (irradiation, air temperature, relative humidity, precipitation, wind velocity)	Hinase: GPV/JMA Meso-scale Spectral Model (MSM)	Japan Meteorological Agency website (http://database.rish.kyoto-u.ac.jp/arch/jmadata/gpv-netcdf.html)
	Shizugawa: Comprehensive Ocean-Atmosphere Data Set (COADS) 2005	Da Silva et al. (1994)
Atmospheric CO_2 concentration	Present: 370 ppm Future: 420 ppm (RCP 2.6 scenario) 900 ppm (RCP 8.5 scenario)	van Vuuren et al. (2011)
Dissolved oxygen (DO) Nutrients (NO_3, PO_4, Si)	Hinase: Public water area water quality measurement data	Ministry of the Environment Website (https://water-pub.env.go.jp/water-pub/mizu-site/mizu/kousui/dataMap.asp)
	Shizugawa: World Ocean Atlas 2009	Garcia et al. (2010a, 2010b)
Total alkalinity (TA)	Present: obtained from the following equation: DIC = 2319 + 0.5155 T – 0.2367 DO where T: water temperature; DO: dissolved oxygen concentration Future: assume that the alkalinity does not change from present	Watanabe et al. (2020)
Dissolved inorganic carbon (DIC)	Present: obtained from the following equation: DIC = 2407 – 12.20 T – 0.7851 DO	Lewis et al. (1998) Watanabe et al. (2020)
	Future: outputs from Model description and results of CMIP5-20c3m experiments (MIROC-ESM) (2086-2095)	Watanabe et al. (2011)

Table 2: End and start dates of Pacific oyster (*C. gigas*) spawning in Hinase and Shizugawa, estimated from observed present and modeled present and future water temperatures and based on Oizumi et al. (1971).

			Hinase		Shizugawa	
			End date	**Start date**	**End date**	**Start date**
Observation			October 24-November 4 (2020) October 25-November 7 (2021)	June 8-19 (2021)	October 8-10 (2020) October 16-18 (2021)	July 19-24 (2021)
Model	**Present**	**Model (present)**	October 24	June 14	October 14	July 26
	2090s	**RCP 2.6**	October 24	June 2	October 24	July 17
		RCP 8.5	November 11	May 18	November 22	?

Table 3: Simulated numbers of days when DO and Ω_{arag} values were below the lower bound of the optimal range (< 203 µmol kg^{-1}; Hochachka, 1980; Fisheries Agency, 2013) and the threshold of acidification (Ω_{arag} < 1.5; Waldbusser et al., 2015) for Pacific oyster larvae in Hinase and Shizugawa. Numbers in parantheses for the threshold of acidification denote the numbers of days of overlap with the Pacific oyster spawning period (except for the 2090s with the RCP 8.5 scenario in Shizugawa, because the spawning period could not be identified).

Threshold			Hinase (# of days)	Shizugawa (# of days)
DO < 203 (µmol kg^{-1})	Present		1	0
	2090s	RCP 2.6	14	0
		RCP 8.5	38	0
Ω_{arag} < 1.5	Present		3 (3)~~0 (0)~~	7 (1)~~0 (0)~~
	2090s	RCP 2.6	5 (5)~~0 (0)~~	7 (1)~~0 (0)~~
		RCP 8.5	256 (69)~~204 (17)~~	322 (?)~~244 (?)~~

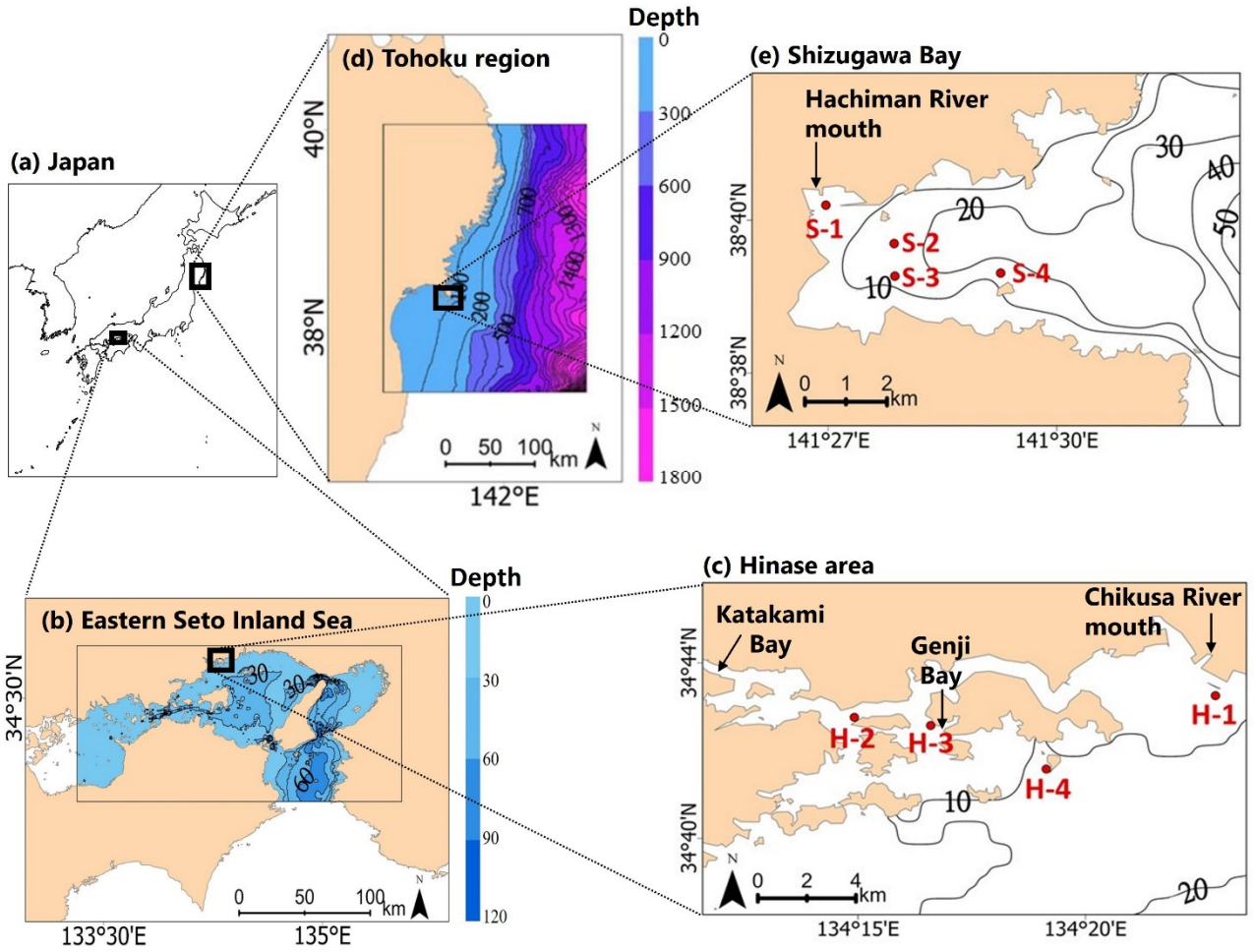

Figure 1: Map of (a) Japan, (b) Eastern Seto Inland Sea, (c) Hinase area, (d) Tohoku region, and (e) Shizugawa Bay. H-1, H-2, H-3, and H-4 in (c) and S-1, S-2, S-3, and S-4 (e) are monitoring sites in Hinase area and Shizugawa Bay, respectively. The extent of the model grids used in each study area are also shown in (b) and (d).

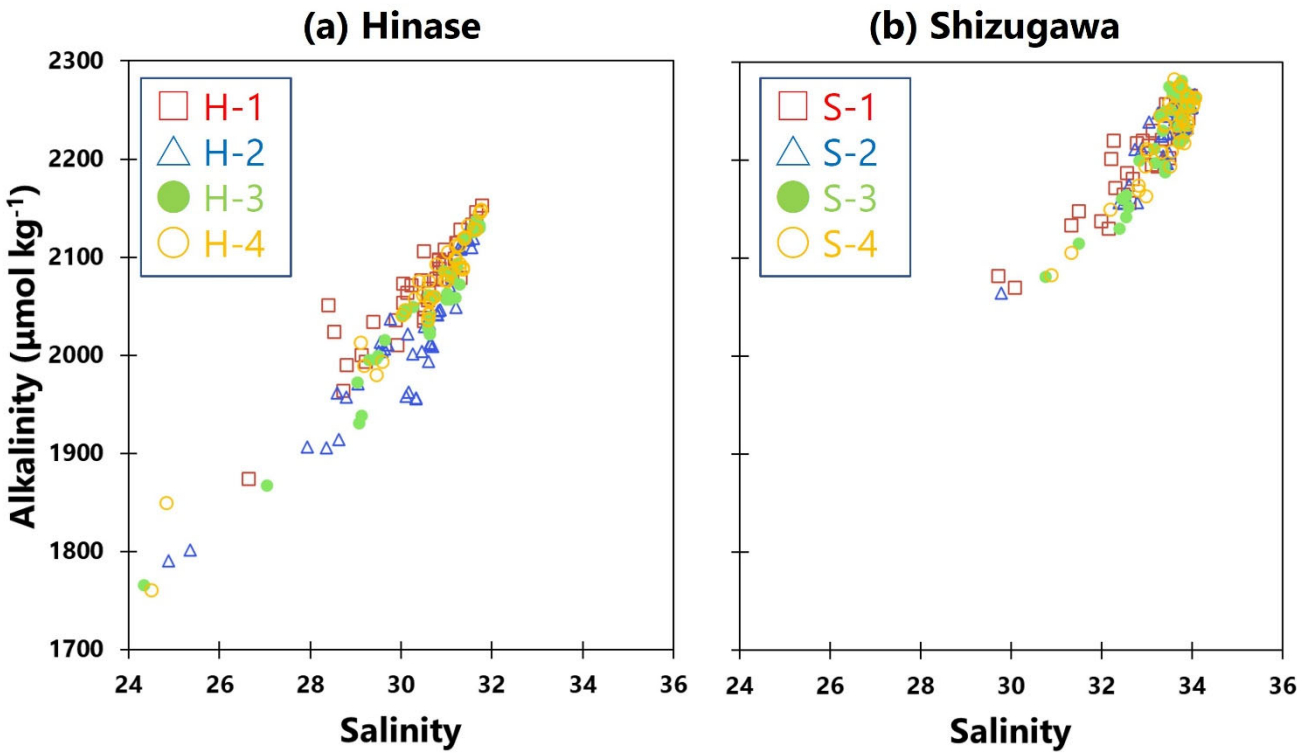

800 **Figure 2: Observed total alkalinity (TA) vs. salinity in (a) Hinase (H-1 [red open square], H-2 [blue open triangle], H-3 [green solid circle], and H-4 [orange open circle]) and (b) Shizugawa (S-1 [red open square], S-2 [blue open triangle], S-3 [green solid circle], and S-4 [orange open circle]). Correlation coefficients: H-1: R^2 = 0.86, H-2: R^2 = 0.85, H-3: R^2 = 0.92, H-4: R^2 =0.94, S-1: R^2 = 0.88, S-2: R^2 = 0.85, S-3: R^2 = 0.90, and S-4: R^2 = 0.90.**

805

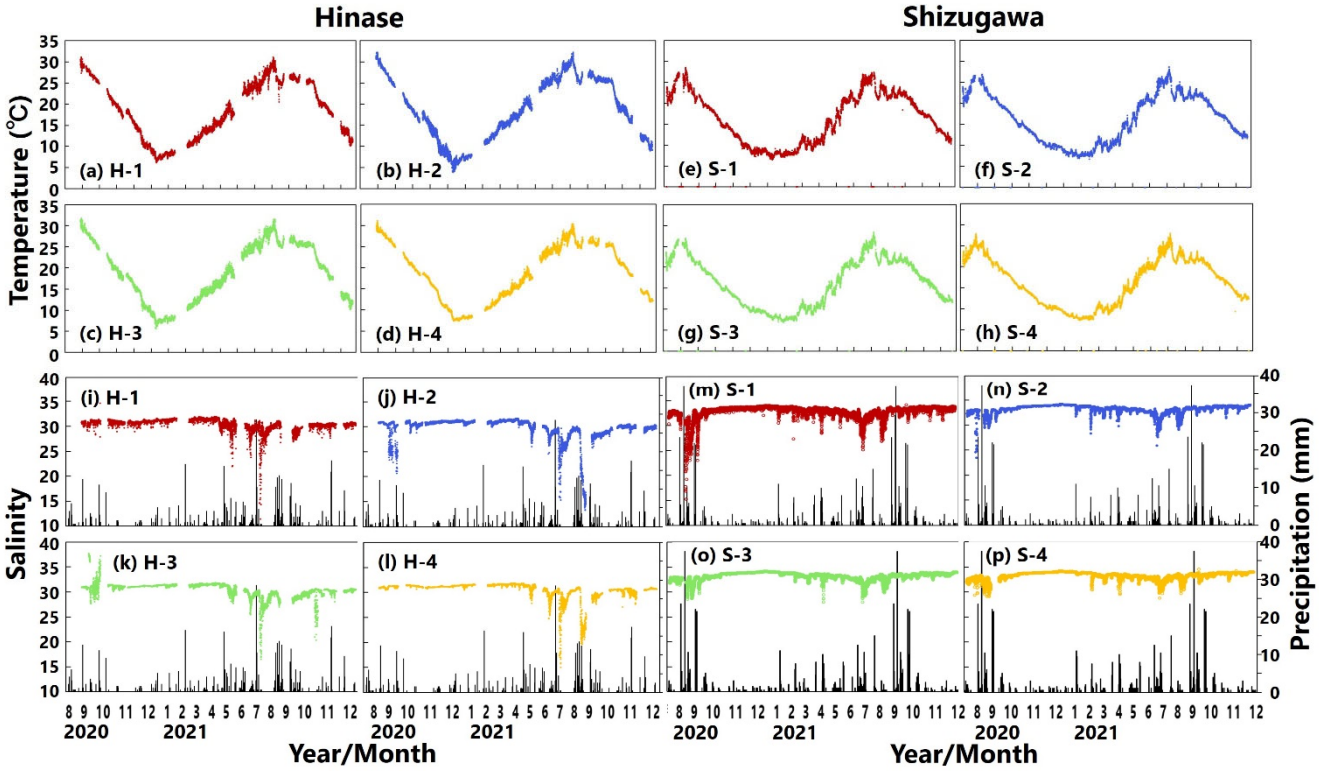

Figure 3: Observed temperature (℃) (top; (a)-(h)) and salinity (bottom; (i)-(p)) values in Hinase (H-1, H-2, H-3, and H-4), and Shizugawa (S-1, S-2, S-3, and S-4) from August 2020 to December 2021. Black bars in (i)-(p) indicate hourly precipitation (mm) at the nearest Automated Meteorological Data Acquisition System (AMeDAS) station—Mushiage (Hinase) and Shizugawa (Shizugawa) (Japan Meteorological Agency website; https://www.data.jma.go.jp/obd/stats/etrn/index.php).

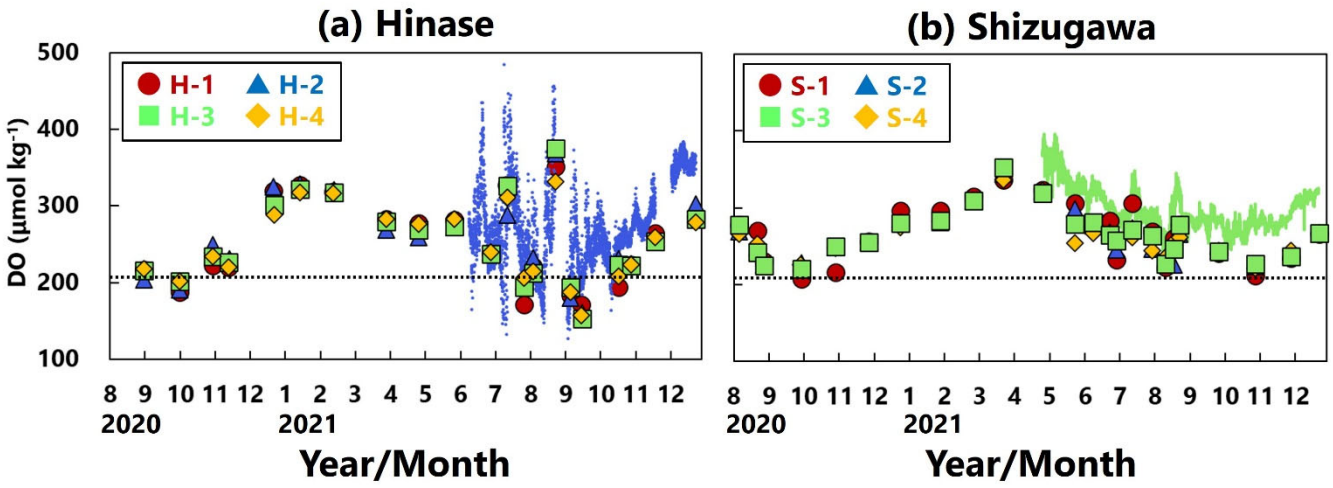

Figure 4: Time series of dissolved-oxygen (DO; µmol kg^{-1}) values in (a) Hinase and (b) Shizugawa. Measurements were carried out when water-bottle samples were collected, and red solid circles (H-1 and S-1), blue solid triangles (at H-2 and S-2), green solid squares (H-3 and S-3), and yellow solid diamonds (H-4 and S-4) are measured values. Continuous monitoring using sensors was performed after June 10, 2021 at H-2 (in blue dots) and after April 27, 2021 at S-3 (in green dots). The monitored values are shown as dots (blue at H-2 and green at S-3). The lower threshold of the optimal DO range for the growth of Pacific oyster (*C. gigas*) (203 µmol kg^{-1}; Hochachka, 1980; Fisheries Agency, 2013) is denoted by a dotted line.

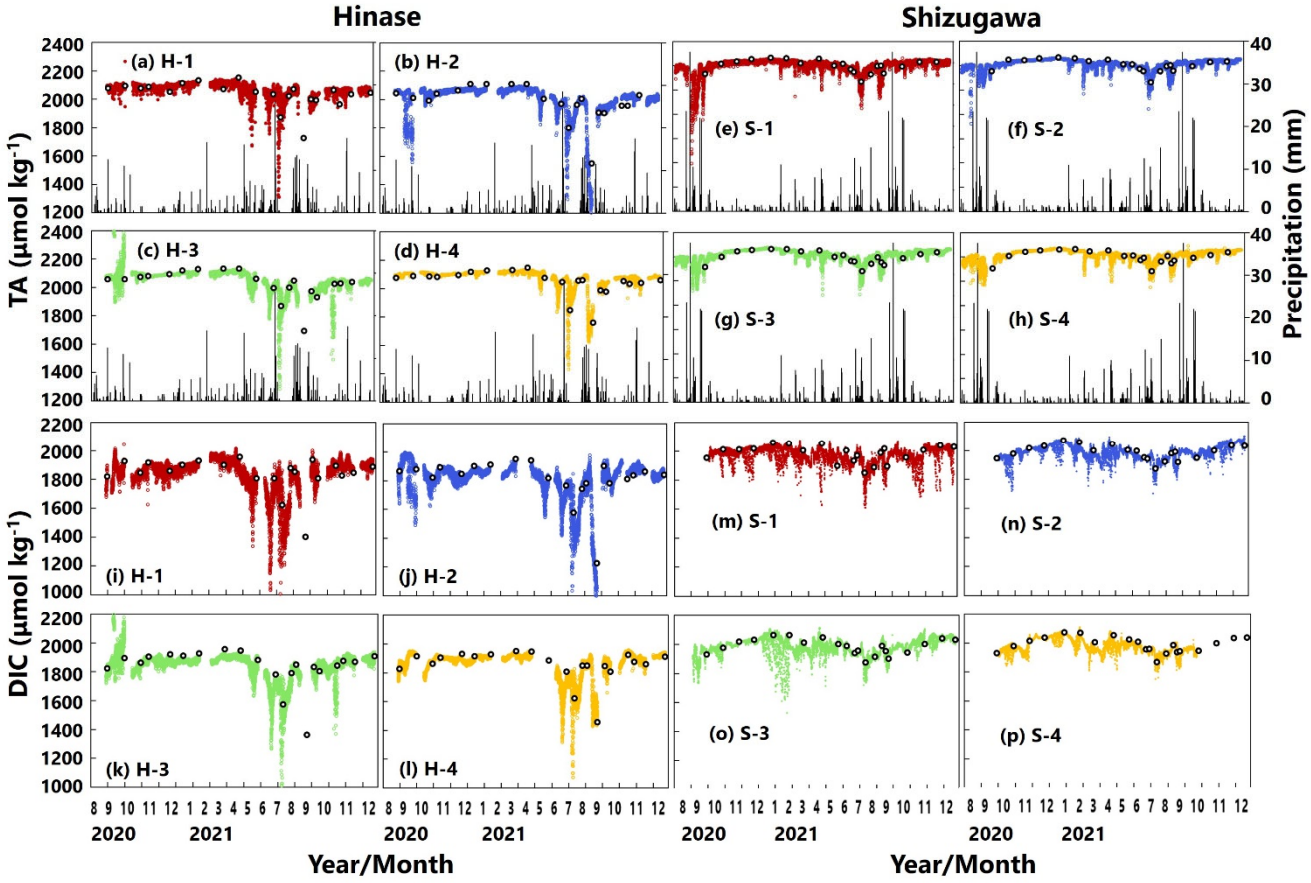

Figure 5: Total alkalinity (TA (μmol kg^{-1}); (a)-(h)) and dissolved inorganic carbon (DIC (μmol kg^{-1}); (i)-(p)) values based on water-sample analysis (open circles) and estimated from continuously observed salinity (colored dots) in Hinase (H-1 to H-4) and Shizugawa (S-1 to S-4) from August 2020 to December 2021. Black bars in (a)-(h) indicate hourly precipitation (mm) at the nearest AMeDAS stations (Japan Meteorological Agency website; https://www**.data.jma.go.jp/obd/stats/etrn/index.php).**

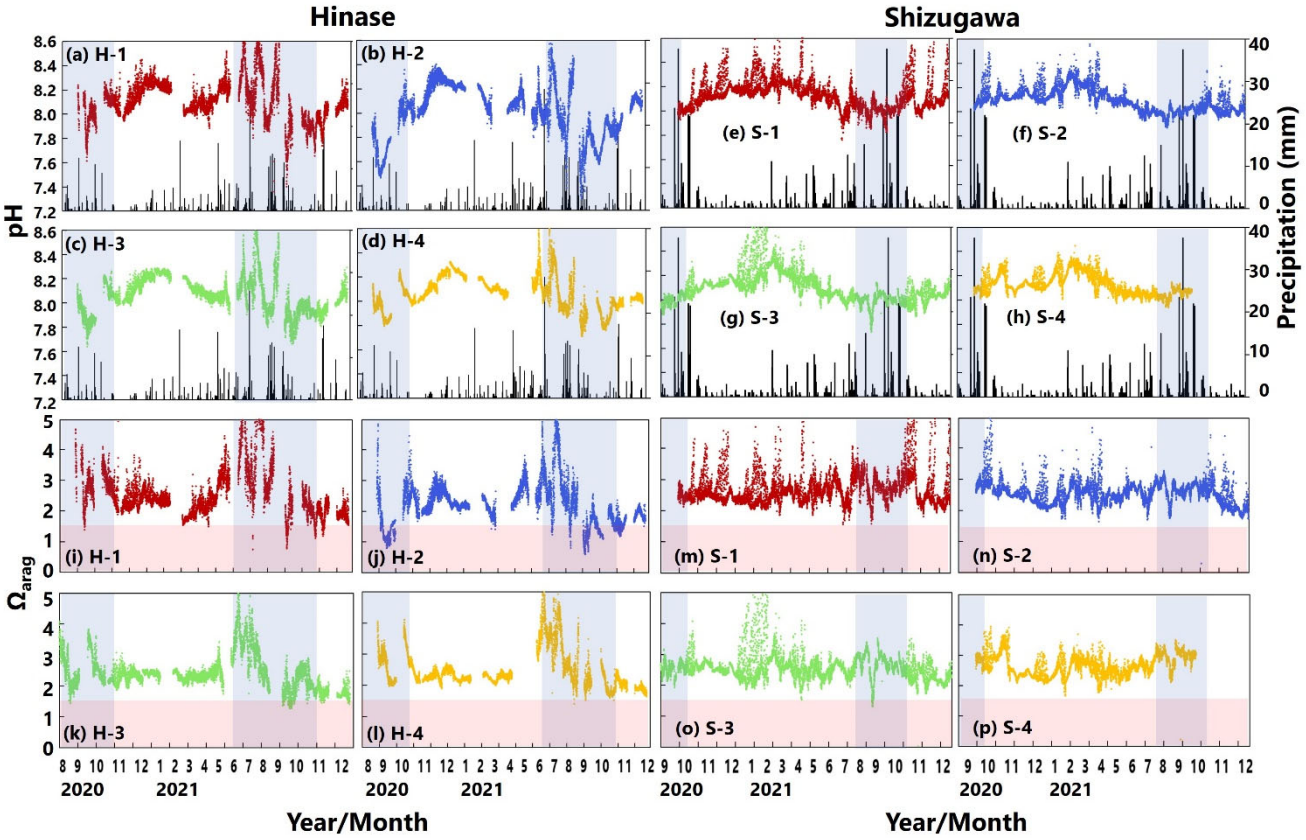

Figure 6: Observed pH ((a)-(h)) and aragonite saturation state (Ω_{arag}) ((i)-(p)) in (a) Hinase (H-1, H-2, H-3, and H-4) and (b) Shizugawa (S-1, S-2, S-3, and S-4) from August or September 2020 to December 2021. Red domains denote the critical level of acidification for Pacific oyster larvae in Waldbusser et al. (2015) ($\Omega_{arag} < 1.5$). Blue domains denote the spawning season of Pacific oyster estimated from Oizumi et al. (1971). Black bars in (a)-(h) indicate hourly precipitation (mm) at the nearest AMeDAS stations (Japan Meteorological Agency website; https://www.data.jma.go.jp/obd/stats/etrn/index.php).

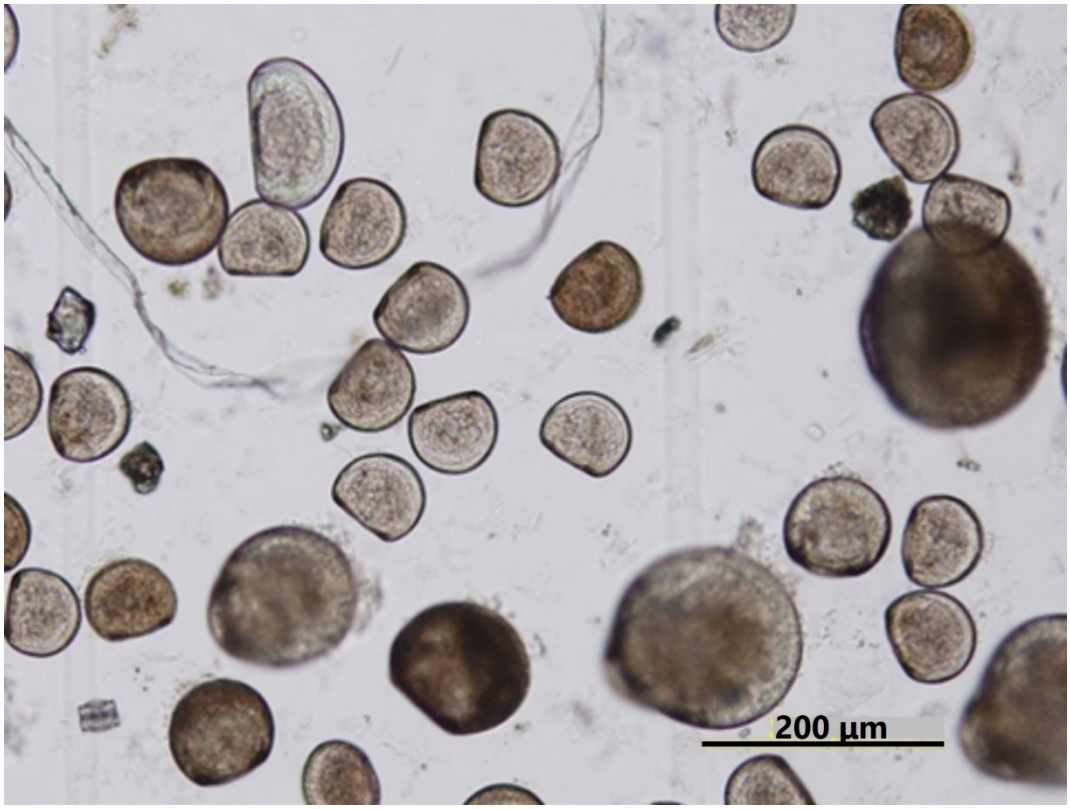

Figure 7: Micrograph of Pacific oyster larvae in Hinase. No morphological abnormalities were observed.

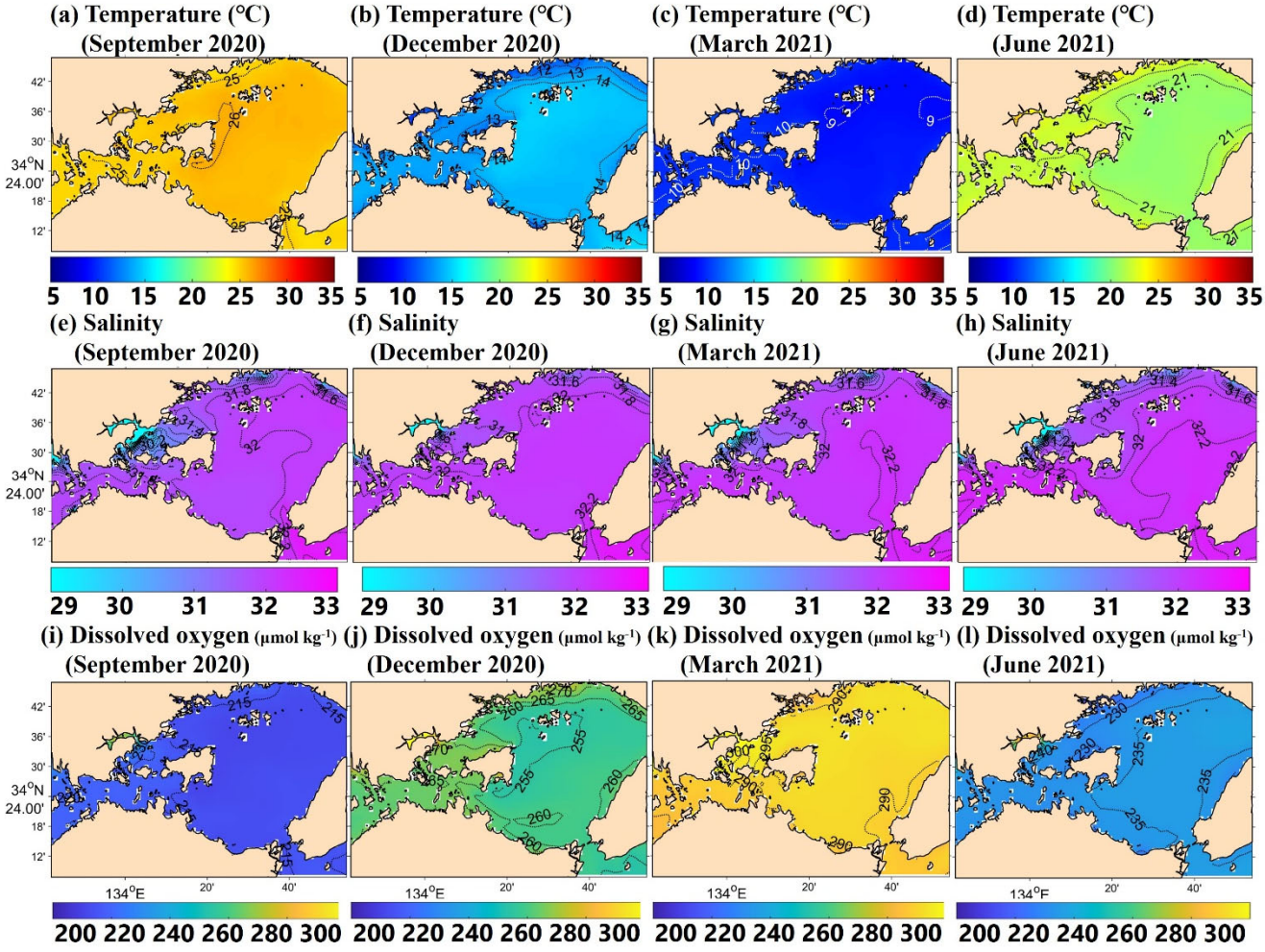

855

Figure 8: Horizontal distribution of modeled monthly-mean surface temperature (℃) ((a)-(d)), salinity ((e)-(h)) and DO (μmol kg^{-1}; (i)-(l)) in September, December, March and June in the model domain of Hinase Area.

860

865

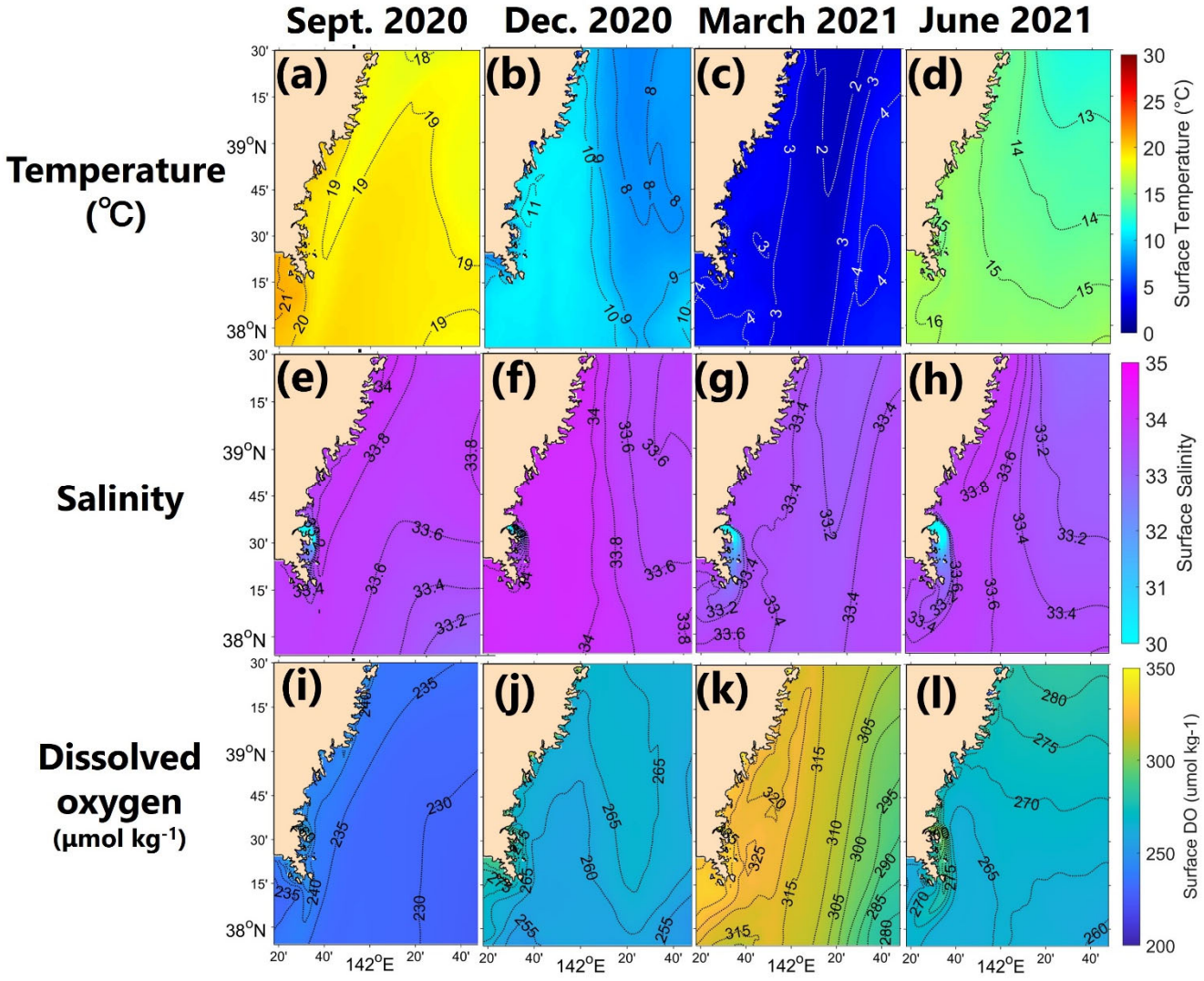

Figure 9: Horizontal distribution of modeled monthly-mean surface temperature (℃) ((a)-(d)), salinity ((e)-(h)) and DO (μmol kg^{-1}; (i)-(l)) in September, December, March and June in the model domain of Shizugawa Bay.

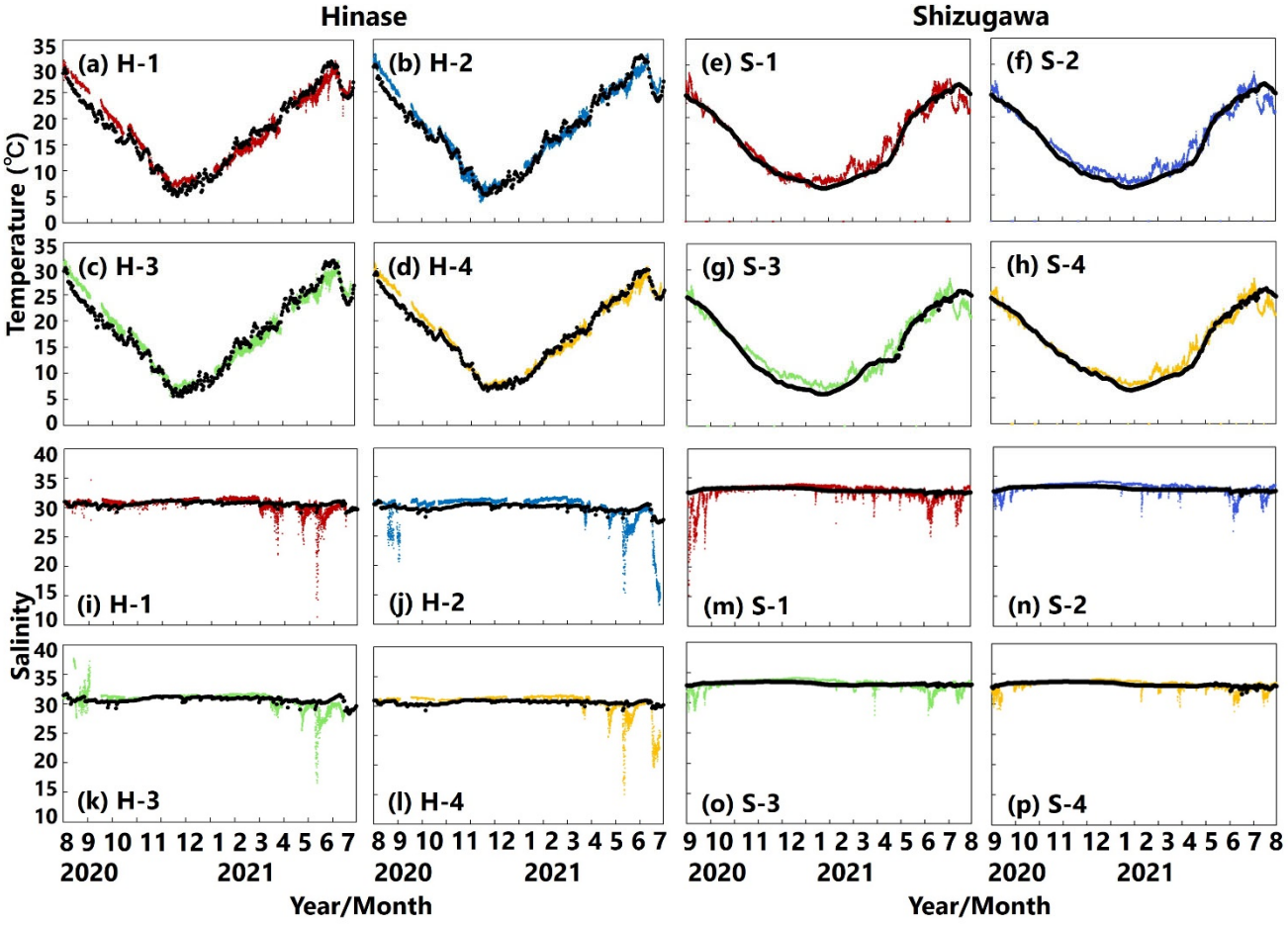

875 **Figure 10: Observed (colored dots) and modeled (black lines) water-temperature ((a)-(h)) and salinity ((i)-(p)) at 1-m depth in Hinase (August 2020 to July 2021) and Shizugawa (September 2020 to August 2021).**

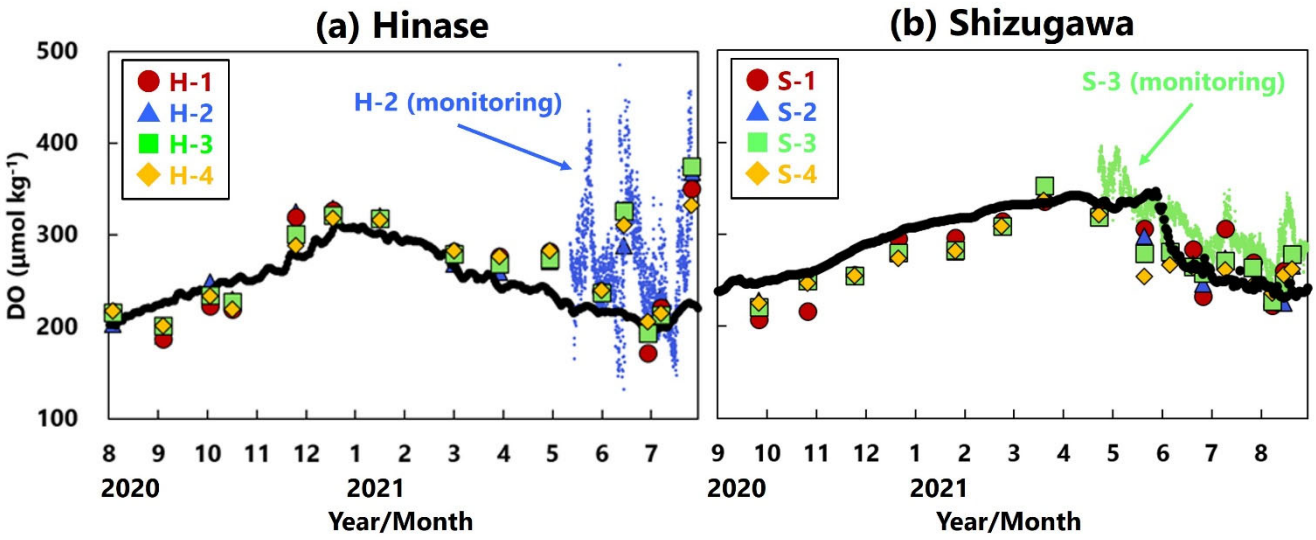

880 **Figure 11: Observed (red circles (H-1 and S-1), blue triangles (H-2 and S-2), green squares (H-3 and S-3), and orange diamonds (H-4 and S-4)) and modeled (black lines) DO concentration (μmol kg^{-1}) at 1-m depth in (a) Hinase (August 2020 to July 2021) and (b) Shizugawa (September 2020 to August 2021). The monitored values are shown as dots (blue at H-2 and green at S-3).**

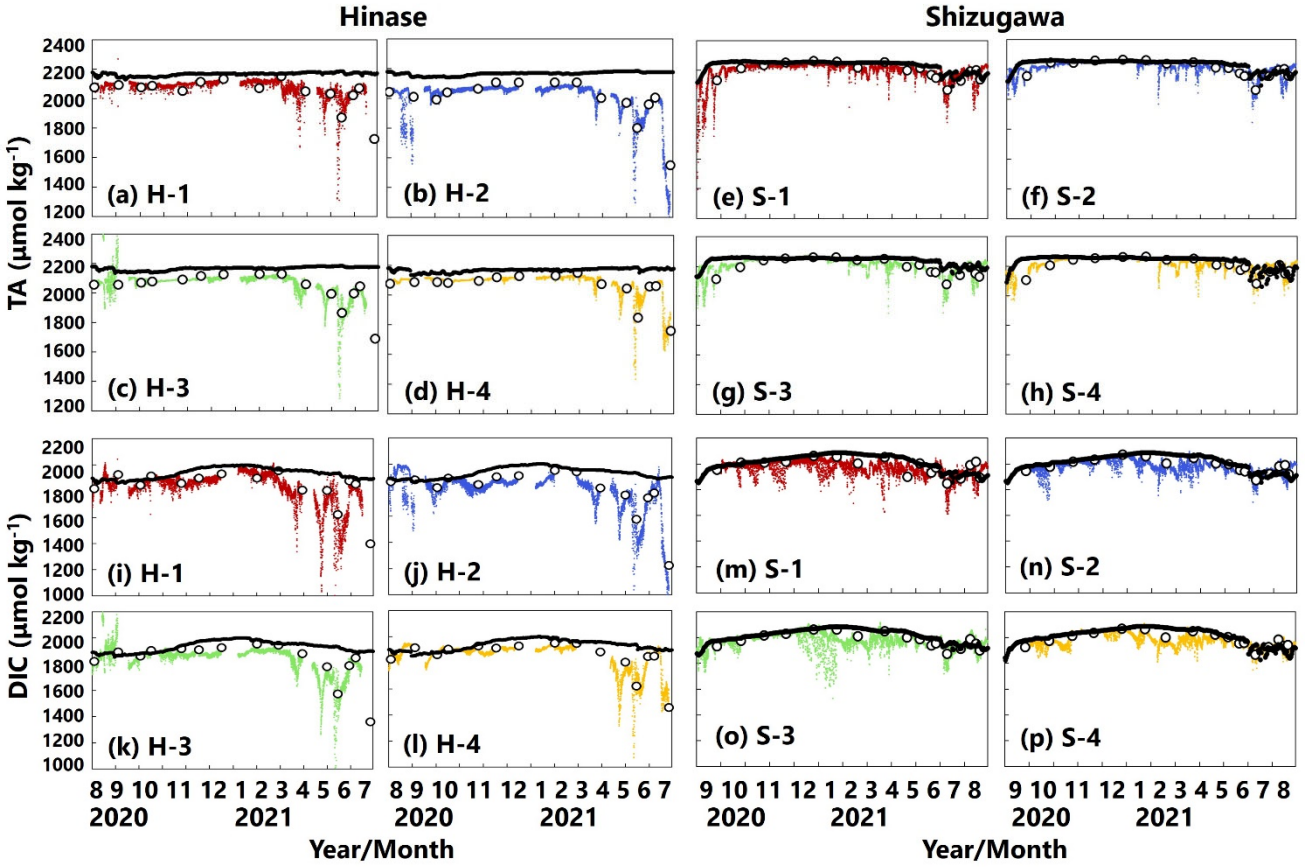

885

Figure 12: Observed (colored dots) and modeled (black lines) TA ((a)-(h); μmol kg^{-1}) and DIC ((i)-(p); μmol kg^{-1}) concentration at 1-m depth in Hinase (August 2020 to July 2021) and Shizugawa (September 2020 to August 2021).

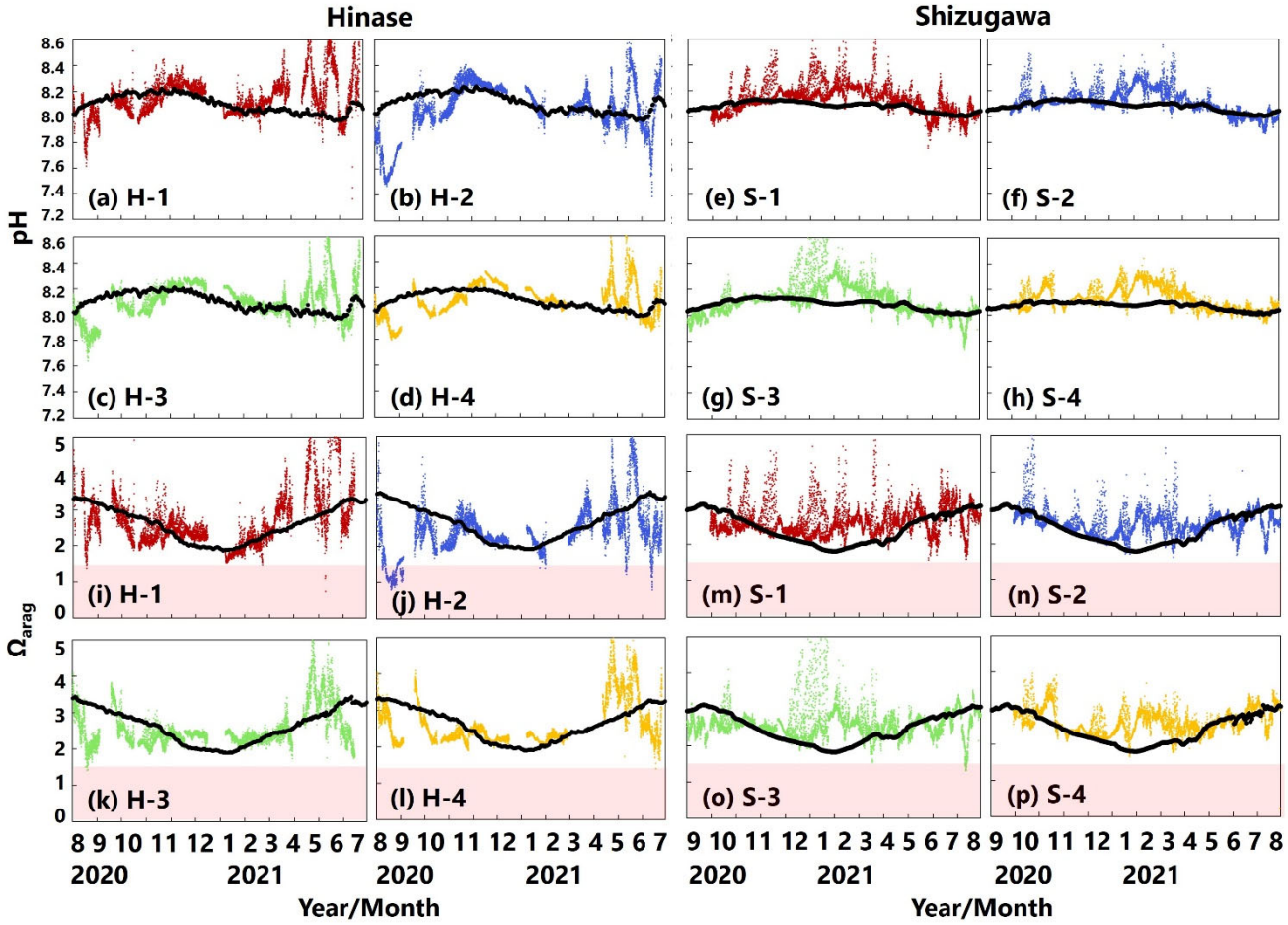

Figure 13: Observed (colored dots) and modeled (black lines) pH ((a)-(h)) and Ω_{arag} ((i)-(p)) at 1-m depth in Hinase (August 2020 to July 2021) and Shizugawa (September 2020 to August 2021). Red domains denote the critical level of acidification for Pacific oyster larvae in Waldbusser et al. (2015) ($\Omega_{arag} < 1.5$).

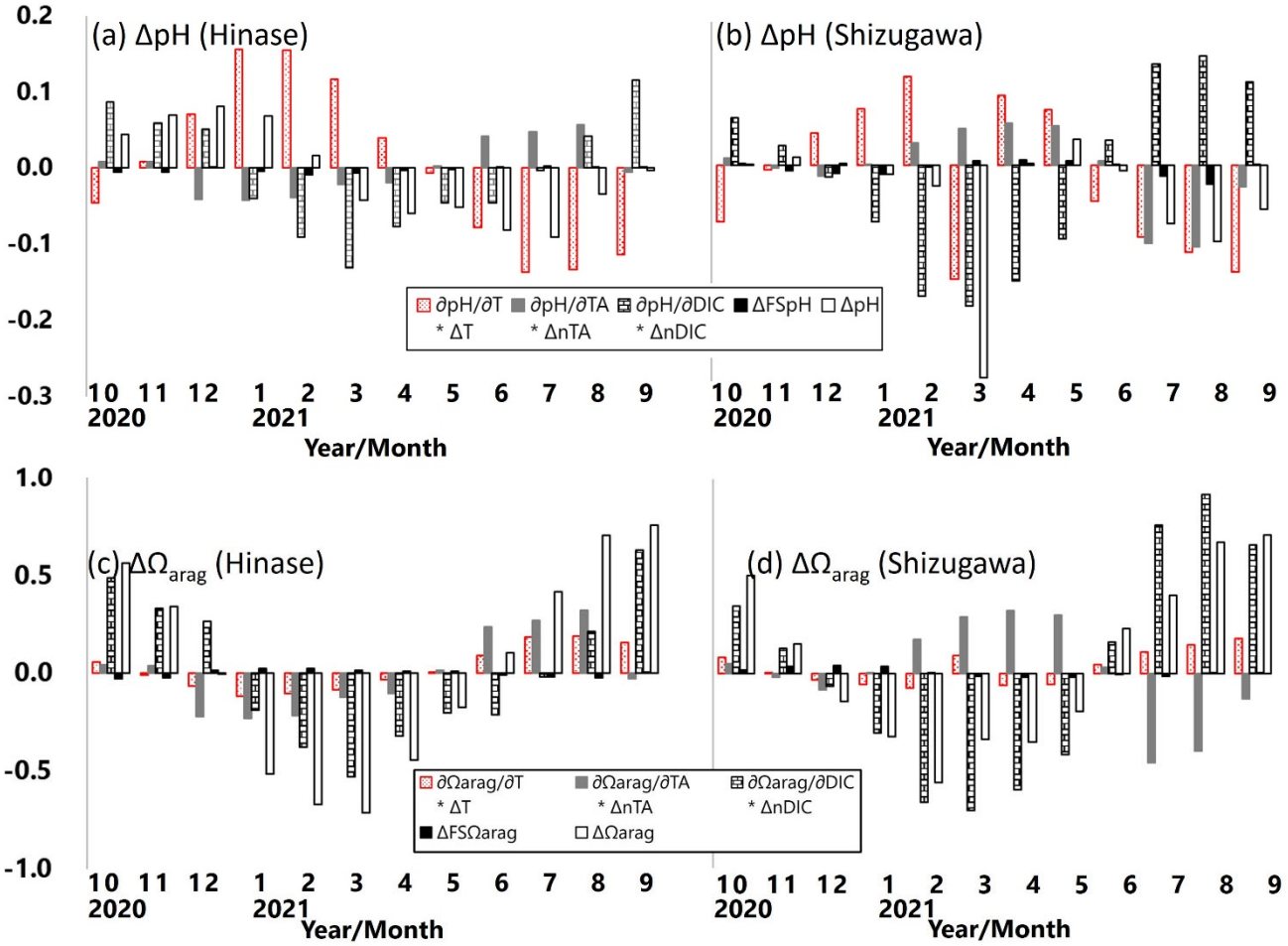

Figure 14. Monthly-mean contributions of pH and Ω_{arag} changes (ΔpH; (a)-(b)) and $\Delta\Omega_{arag}$; (c)-(d), respectively) in temperature (∂ pH/∂ T * ΔT and $\partial\Omega_{arag}$ /∂T * ΔT), TA (∂pH/∂T * ΔT and $\partial\Omega_{arag}$ /∂T * ΔT), DIC (∂pH/∂T * ΔT and ∂ Ω_{arag} /∂T * ΔT), and salinity (ΔFSpH and ΔFSΩ_{arag}) in Hinase ((a), (c)) and Shizugawa ((b), (d)).

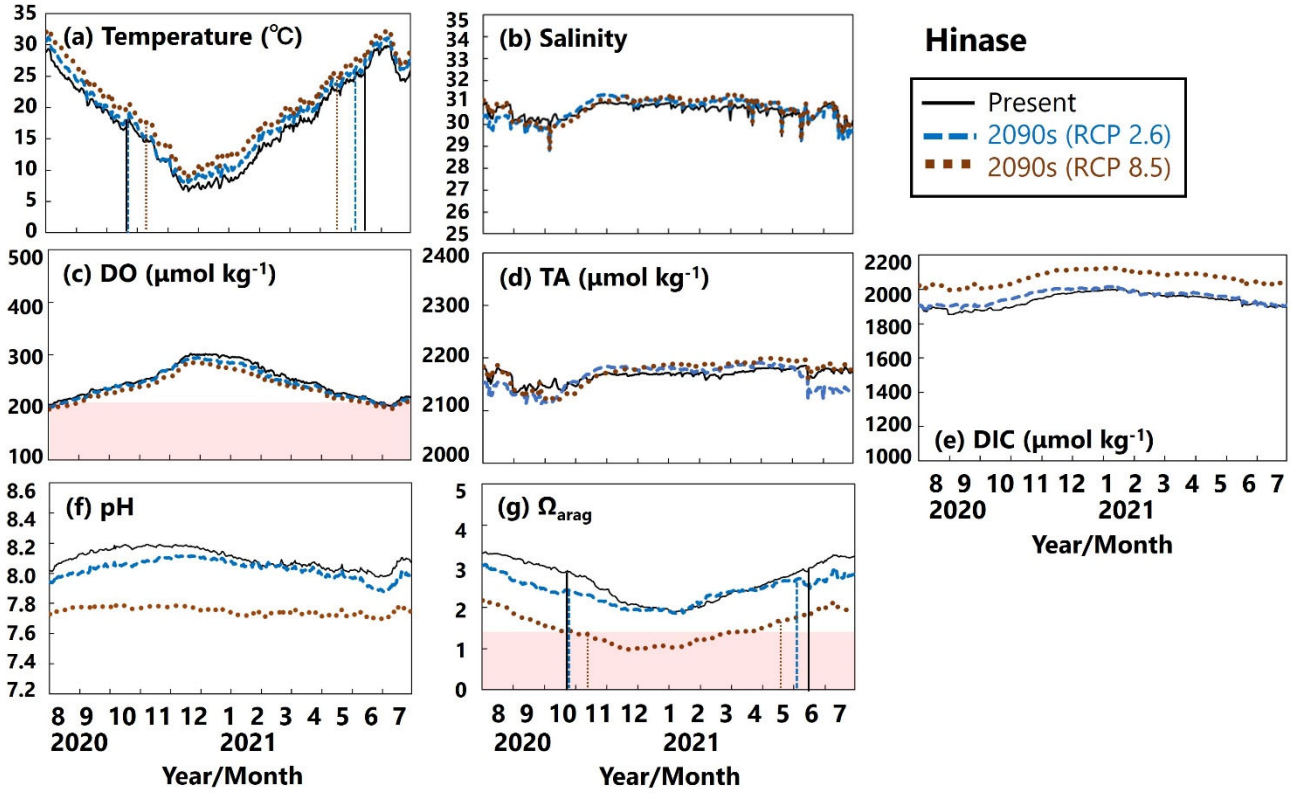

Figure 15: Modeled (a) temperature (°C), (b) salinity, (c) DO (µmol kg^{-1}), (d) TA (µmol kg^{-1}), (e) DIC (µmol kg^{-1}), (f) pH, and (g) Ω_{arag} values in Hinase from August to July currently (black solid lines) and in the 2090s (RCP 2.6 scenario, blue dashed lines; RCP 8.5 scenario, brown dotted lines). Red domain in (c) denotes DO concentrations below the optimum DO range (< 203 µmol kg^{-1}) for the growth of Pacific oyster (Hochachka, 1980; Fisheries Agency, 2013). Red domain in (g) denotes the critical level of acidification for Pacific oyster larvae in Waldbusser et al. (2015) (Ω_{arag} < 1.5). Modeled end and start dates of spawning period of Pacific oysters at present and in 2090s with RCP 2,6 and 8.5 scenarios (Table 2) are shown in vertical solid black lines, dashed blue lines, and dotted brown lines, respectively, in (a) and (g). The end and start dates of the spawning period were estimated by referring to thresholds obtained from Oizumi et al. (1971).

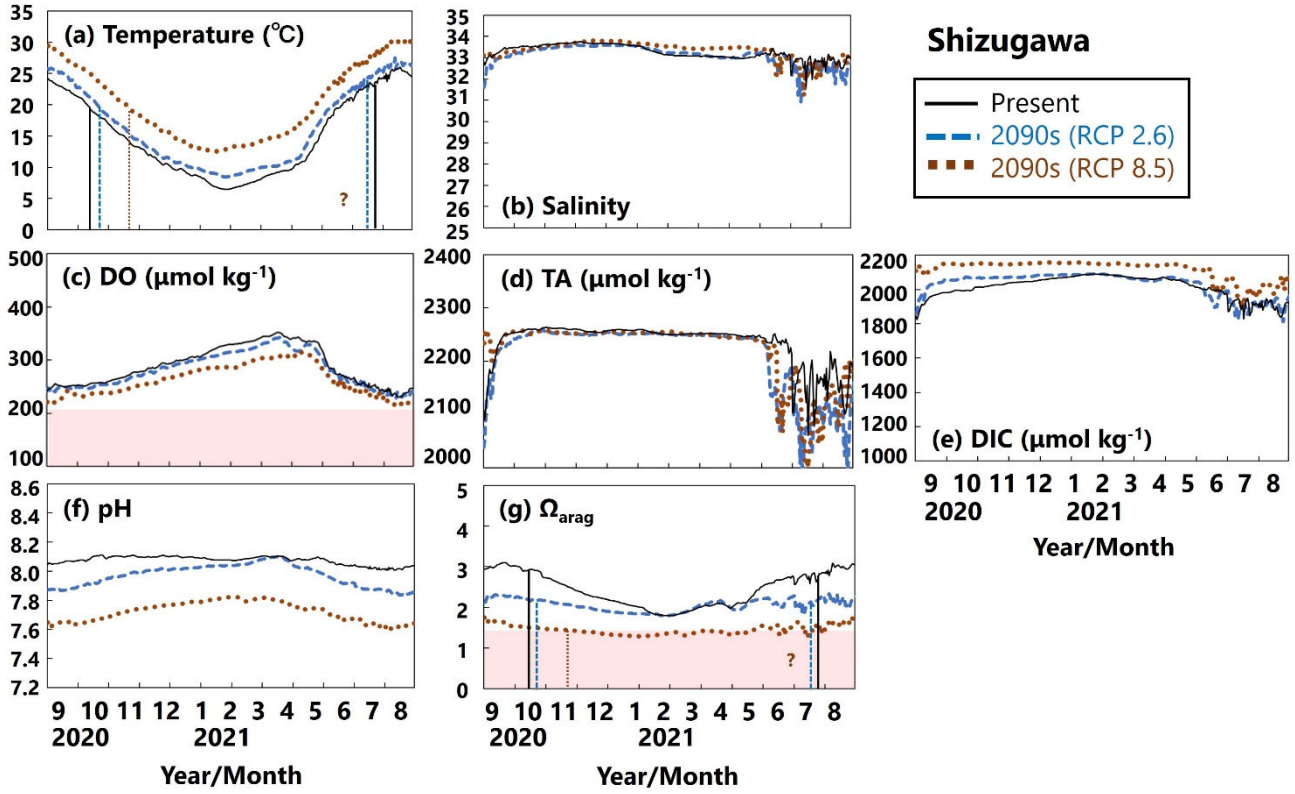

Figure 16: Modeled (a) temperature (°C), (b) salinity, (c) DO (µmol kg^{-1}), (d) TA (µmol kg^{-1}), (e) DIC (µmol kg^{-1}), (f) pH, and (g) Ω_{arag} values in Shizugawa from September to August currently (black solid lines) and in the 2090s (RCP 2.6 scenario, blue dashed lines; RCP 8.5 scenario, brown dotted lines). Red domain in (c) denotes DO concentrations below the optimum DO range (< 203 µmol kg^{-1}) for the growth of Pacific oyster (Hochachka, 1980; Fisheries Agency, 2013). Red domain in (g) denotes the critical level of acidification for Pacific oyster larvae in Waldbusser et al. (2015) (Ω_{arag} < 1.5). Modeled end and start dates of spawning period of Pacific oysters at present and in 2090s with RCP 2,6 and 8.5 scenarios (Table 2) are shown in vertical solid black lines, dashed blue lines, and dotted brown lines, respectively, in (a) and (g). The end and start dates of the spawning period were estimated by referring to thresholds obtained from Oizumi et al. (1971). The start date of the spawning season in 2090s with RCP 8.5 scenario could not be projected in Shizugawa because water temperature lower than 10 °C was not projected, and therefore, the threshold for evaluating the start date by Oizumi et al. (1971) could not be applied.

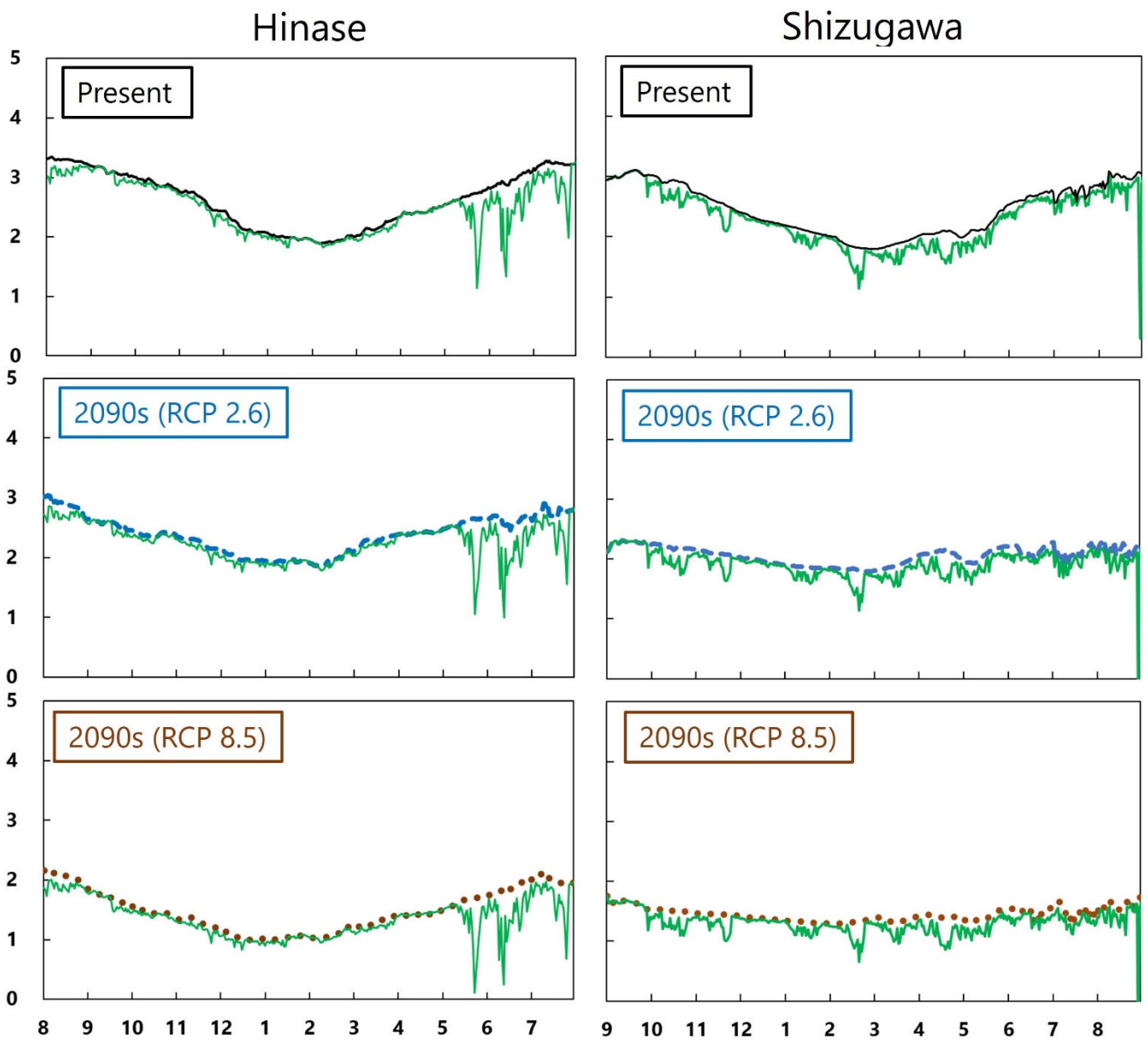

Figure S1. Simulated or projected Ω_{arag} in Hinase from August to July (left) and in Shizugawa from September to August (right) for the~~at~~ present (top), for the~~in~~ 2090s with the RCP 2.6 scenario (middle), and for the~~in~~ 2090s with the RCP 8.5 scenario (bottom). Solid black lines, dashed blue lines, and dotted brown lines are identical to results shown in Figures 15(g) and 16(g). Solid green lines denote modeled daily Ω_{arag} minima if present day observed daily Ω_{arag} fluctuations ~~at present~~ are~~is applied~~included.